EUROPEAN ORGANIZATION FOR NUCLEAR RESEARCH (CERN)

# The LHCb Upgrade

Jaap Panman
CERN
*For the LHCb Collaboration*

*This document reproduces the relevent pages of the LHCb Upgrade LOI, CERN/LHCC/2011-001*

contribution to HEPMAD-11
13 October 2011

**Abstract**

The primary goal of LHCb is to measure the effects of new particles or forces beyond the Standard Model. Results obtained from data collected in 2010 and 2011 show that the detector is robust and functioning well. While LHCb will be able to measure a host of interesting channels in heavy flavour decays in the upcoming few years, a limit of about 1 $\text{fb}^{-1}$ of data per year cannot be overcome without upgrading the detector. The LHC machine does not face such a limitation. With the upgraded detector, read out at 40 MHz, a much more flexible software-based triggering strategy will allow a large increase not only in data rate, as the detector would collect 5 $\text{fb}^{-1}$ per year, but also the ability to increase trigger efficiencies especially in decays to hadronic final states. In addition, it will be possible to change triggers to explore different physics as LHC discoveries point us to the most interesting channels. Our physics scope extends beyond that of flavour. Possibilities for interesting discoveries exist over a whole variety of phenomena including searches for Majorana neutrinos, exotic Higgs decays and precision electroweak measurements. Here we describe the physics motivations and proposed detector changes for exploring new phenomena in proton-proton collisions near 14 TeV centre-of-mass energy.

# Chapter 1

# Introduction

## 1.1 Flavour physics in the era of the LHC

Studies of hadronic flavour physics observables have provided critical input in the construction of the Standard Model (SM). Flavour measurements provided the first indications of the existence and nature of the charm quark, the third generation, and the high mass scale of the top. In searching for physics beyond the Standard Model it is also evident that flavour observables will play a central role.

Many of the open questions of the SM are associated with the flavour sector. Why are there three generations (if there are only three)? What determines the hierarchy of quark masses? What is responsible for the characteristic structure of the CKM matrix? Furthermore, two of the very few observations that cannot be accommodated in the Standard Model, namely the baryon-antibaryon asymmetry of the universe, and non-zero neutrino mass, are of a flavour physics nature.

Flavour physics measurements already exert significant weight in limiting the parameter space of New Physics (NP) beyond the SM. The strongest constraints on supersymmetric Higgs bosons come not from direct searches, but from limits on, and measurements of, the rates of suppressed heavy flavour decays such as $B_s \to \mu^+\mu^-$, $b \to s\gamma$ and $B^- \to \tau^-\nu$. These observables will continue to have great importance in the era of the LHC. This can be seen in Fig. 1.1, which illustrates for a popular variant of SUSY (NUHM1 [1]), how measurements that are sensitive to values of $\mathcal{B}(B_s \to \mu^+\mu^-)$ below $1 \times 10^{-8}$ have greater discovery power over the parameter space indicated than direct searches for the $H$ and $A$ Higgs bosons performed with up to 60 fb$^{-1}$ [2]. Moreover, a measurement of $\mathcal{B}(B_s \to \mu^+\mu^-)$ together with any direct observation of a $H$ or $A$ candidate will be invaluable in elucidating the nature of the underlying physics.

The physics opportunities of the LHC in terms of direct searches are well known; its potential in flavour physics through the enormous production rate of $B$ and $D$ hadrons is no less rich. At the LHC observation of $B_s \to \mu^+\mu^-$ and other rare decays will be possible, as well as detailed studies of important kinematical distributions that have not been accessible at previous facilities, such as the angular distribution of the decay products in $B^0 \to K^*\mu^+\mu^-$, which are highly sensitive to the helicity structure of any NP effects [4].

A particular attraction of performing flavour physics at the LHC is the opportunity to make measurements of $CP$-violating asymmetries with much higher precision than has been possible

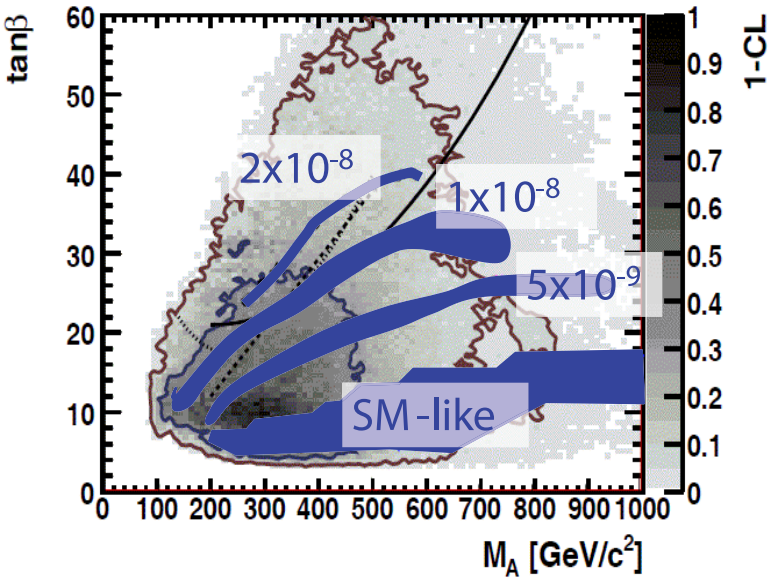


Figure 1.1: The correlations between the preferred values of $M_A$ and $\tan\beta$ in the NUHM1 variant of MSSM [3]. Superimposed are the contours indicating the value of $\mathcal{B}(B_s \to \mu^+\mu^-)$ in this framework. Also indicated are the $5\,\sigma$ discovery contours for observing the heavy MSSM Higgs bosons $H$, $A$ in the decay channels $H, A \to \tau^+\tau^-$ jets (solid line), jet + $\mu$ (dashed line), jet + $e$ (dotted line) assuming an analysis requiring 30 or 60 fb$^{-1}$ collected with the CMS detector [2].

hitherto. These asymmetries are a priori very sensitive to the contribution from NP effects. It is therefore surprising that the measurements of $CP$ violation performed with $B^0$ and $B^\pm$ mesons at BABAR and Belle are broadly consistent with the CKM mechanism of the SM [5,6]. If new particles exist at the TeV mass scale, as is expected, then this is already an indication that the flavour couplings of the NP have a very particular structure, so as not to have given rise to effects inconsistent with the SM expectations. More precise measurements are needed to test whether the CKM description remains successful at the sub-10% level. Even more exciting is the possibility to extend this programme to the $B_s$ sector, about which very little is known and where more visible effects may be apparent. Recent measurements from the Tevatron hint at larger than expected $CP$ violation in $B_s \to J/\psi\phi$ [7, 8] and in $B_s$ mixing [9, 10], but measurements with higher precision are required to clarify the situation. This will only be possible at the LHC.

## 1.2 LHCb goals with current and upgraded detector

LHCb is an experiment that has been designed to perform flavour physics measurements at the LHC. Its physics programme will be executed in two phases. A full discussion of the goals of each phase may be found in Chapter 2. Here a brief overview is given.

The aims of the first phase of the experiment can be achieved with around 5 fb$^{-1}$ of data and will take several years to accomplish, using the current detector. With this data-set, it will be possible to extend significantly the precision of many key observables in $B$ and $D$ physics beyond what was possible at the B-factories, and make the first exploration of the $B_s$ system.

To exploit fully the flavour-physics potential of the LHC will then require an upgrade to the

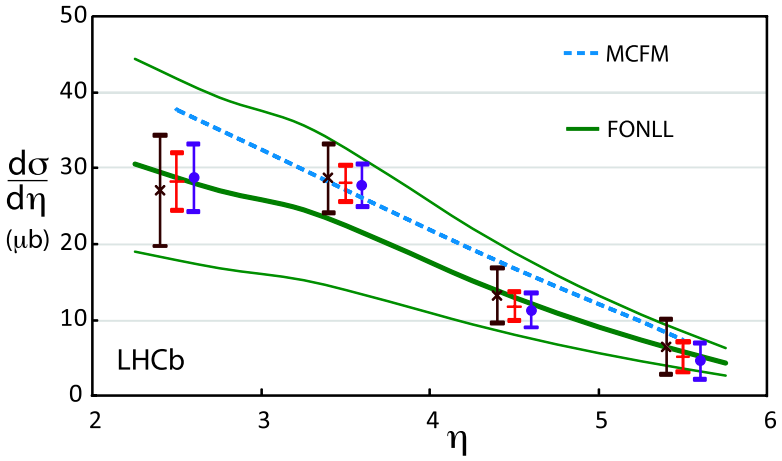


Figure 1.2: LHCb measurement of the $b\bar{b}$ cross-section at $\sqrt{s} = 7$ TeV, as a function of rapidity. In each rapidity bin measurements performed with two sets of trigger conditions are shown (black and blue), which are then averaged together to give the final result (red, with smallest error bars). Also shown are two theoretical predictions [12].

detector, as proposed in this document. The upgrade will allow the experiment to operate at higher luminosity, and will equip the detector with a fully flexible software trigger. This latter attribute will be invaluable for improving the selection efficiency for hadronic final states in $B$ and $D$ decays. The upgraded detector will be able to collect 50 fb$^{-1}$ of data integrated over around ten years of operation.

The aim of both the existing experiment and the upgrade is to search for effects of processes beyond the SM, and to characterise the nature of the underlying physics. In both phases a wide programme of studies will be performed, which can be broadly divided into two equally important categories, as summarised in Table 1.1. In the first category ("Exploration") are those studies which exploit decay modes or observables which are a priori very sensitive to NP, but have not been accessible at previous experiments. The hope here is to observe large non-SM effects. The second category ("Precision Studies") encompasses measurements of known parameters with improved sensitivity, to allow for more precise comparisons with theory. The strategies for performing the studies in certain key topics with the existing detector have been mapped out using simulation [11]. The data collected give confidence that these physics goals are achievable, as it has been observed that the detector is performing as expected and that the cross-section for heavy-flavour production agrees with the theoretical predictions (see Fig. 1.2).

In the physics exploitation of the upgraded experiment the Exploration category will be populated by important new observables and decay modes, which cannot be studied with interesting precision at the existing experiment. This means that the physics gain of the upgrade cannot be assessed by merely applying a '$1/\sqrt{N}$' scaling to the expectations of the current detector. The topics which had been classified in the Exploration category for the existing experiment will migrate to the class of Precision Studies. Improved knowledge of these observables will be essential in understanding the NP which it is hoped that the LHC will uncover.

The potential of LHCb extends far beyond quark flavour physics. Important studies are also possible in the lepton sector, including the search for lepton-flavour violating tau decays and

Table 1.1: LHCb quark flavour physics goals, illustrated with selected examples for the current and upgraded detector.

| | Exploration | Precision studies |
|---|---|---|
| Current LHCb | Search for $B_s \to \mu^+\mu^-$ down to SM value<br><br>Search for mixing induced $CP$ violation in $B_s$ system ($2\beta_s$) down to SM value<br><br>Look for non-SM behaviour in forward-backward asymmetry of $B^0 \to K^*\mu^+\mu^-$<br><br>Look for evidence of non-SM photon polarisation in exclusive $b \to s\gamma^{(*)}$ | Measure unitarity triangle angle $\gamma$ to $\sim 4^\circ$ to permit meaningful CKM tests<br><br>Search for CPV in charm |
| Upgraded LHCb | Search for $B^0 \to \mu^+\mu^-$<br><br>Study other kinematical observables in $B^0 \to K^*\mu^+\mu^-$, e.g. $A_T(2)$<br><br>CPV studies with gluonic penguins e.g. $B_s \to \phi\phi$<br><br>Measure $CP$ violation in $B_s$ mixing ($A^s_{fs}$) | Measure $\mathcal{B}(B_s \to \mu^+\mu^-)$ to a precision of $\sim 10\%$ of SM value<br><br>Measure $2\beta_s$ to precision $< 20\%$ of SM value<br><br>Measure $\gamma$ to $< 1^\circ$ to match anticipated theory improvements<br><br>Charm CPV search below $10^{-4}$<br><br>Measure photon polarisation in exclusive $b \to s\gamma^{(*)}$ to the % level |

for low mass Majorana neutrinos. Furthermore, the forward geometry, precise vertexing and particle identification capabilities of the detector give LHCb unique and exciting possibilities in the areas as diverse as electroweak physics, the search for long-lived new particles, and QCD. In all cases great benefit will come both from the increased sample sizes that will be made available with the upgrade, and the flexible software trigger. More discussion is given to these opportunities in Chapter 2.

## 1.3 Running LHCb with large pile-up

Recent running of LHCb, albeit at luminosities below nominal design, have approached interaction rates per bunch expected at the upgrade. The effect on the detector of much higher number of visible interactions per crossing, $\mu$, than originally planned has therefore been observed. The detector has been run with $\mu$ values of up to 2.5, similar to those expected in the upgrade scenario, while the nominal design value was $\mu = 0.4$. However, an upgraded LHCb

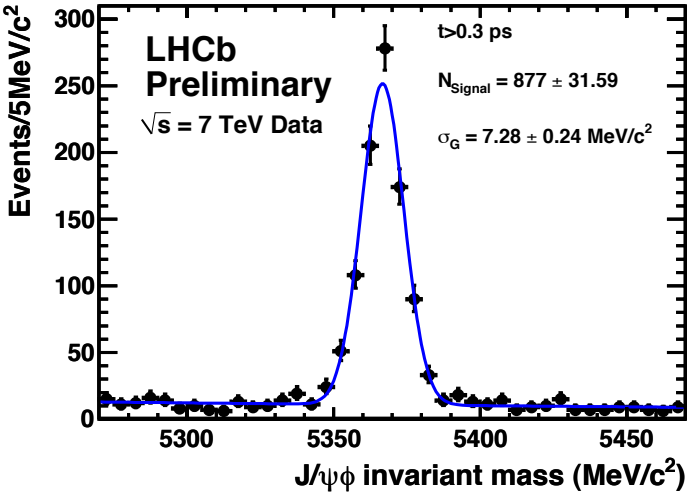


Figure 1.3: Invariant mass distribution of $J/\psi(\mu^+\mu^-)\phi(K^+K^-)$ candidates, using 35 pb$^{-1}$ of data.

detector will experience larger bunch-to-bunch spillover, and track multiplicities will increase somewhat given the expected doubling of the LHC beam energy.

Running at larger than design pile-up results in an increased combinatorial background and lower reconstruction efficiency due to increased occupancy in the detector. Studies of the data suggest that these effects are much smaller than might initially have been expected.

**Impact on combinatorial background** The impact of the large pile-up on the combinatorial background has been studied extensively [11]. The invariant mass of $J/\psi(\mu^+\mu^-)\phi(K^+K^-)$ candidates, which are used to measure the $B_s$ mixing phase, are shown in Fig. 1.3. These candidates have been reconstructed in the data taken in 2010 with an average $\mu = 1.8$. The distribution shows a signal-to-background ratio (S/B) of around 5. This level of background results in only a very small loss in sensitivity compared to that expected in nominal LHCb conditions.

To extrapolate to even larger pile-up, Fig. 1.4 shows S/B extracted from the invariant mass distributions of $J/\psi(\mu^+\mu^-)K^\pm$ candidates as a function of the number of primary vertices (PVs) reconstructed. The S/B of $B_s \to J/\psi(\mu^+\mu^-)K^\pm$ is comparable to that of $B_s \to J/\psi(\mu^+\mu^-)\phi(K^+K^-)$. However, the former decays have an order of magnitude more statistics. This allows the S/B to be investigated in events with up to five PVs. The S/B value is found to be independent of the number of PVs, due to the fact that the separation between PVs is on the order of centimetres, while the resolutions of primary and secondary vertices are $\sim 60$ $\mu$m and $\sim 200$ $\mu$m, respectively. For this core physics channel the LHCb detector therefore performs very well in terms of S/B, even in the presence of large pile-up. For some other channels, for example inclusive semileptonic decays such as $B \to D\mu X$, some degradation is observed.

**Impact on track reconstruction efficiency** To check the track reconstruction efficiency for large pile-up, the data has been used to validate the reconstruction efficiency of charged tracks in Monte-Carlo simulation. The simulation results are in good agreement with the observed

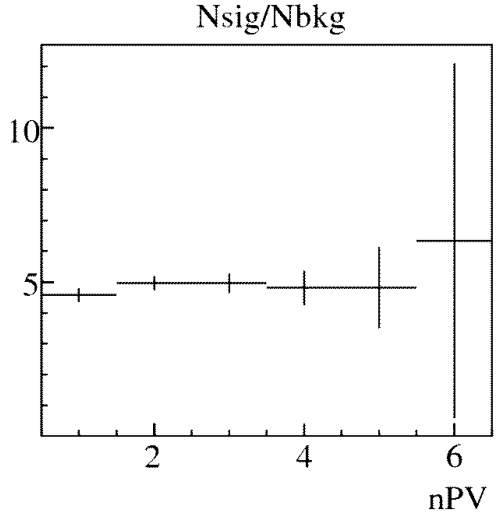


Figure 1.4: Signal-to-background ratio for the invariant mass distribution of $J/\psi(\mu^+\mu^-)K^\pm$ as a function of the number of primary vertices reconstructed in the event.

efficiencies, which gives confidence in using the simulation to determine the maximum pile-up at which the reconstruction of charged tracks would still work with the present LHCb detector.

Owing to the limited number of LHC bunches, LHCb has not yet been exposed to spill-over[1] from neighbouring LHC buckets. With the nominal number of bunches, 2622, the probability that a consecutive crossing also has a $pp$ interaction is 0.33 at $\mu = 0.4$, while at $\mu = 2$ this probability rises to 0.86.

The Outer Tracker subdetector is sensitive to spill-over and from $\mu = 0.4$ to $\mu = 2$ its occupancy rises by a factor two. Other subdetector systems which are less sensitive to spill-over, see the occupancy rise by a factor $\sim$1.6. To test the reconstruction efficiency, crossings have been simulated containing $B_s \to \phi(K^+K^-)\phi(K^+K^-)$ decays, and the efficiency to reconstruct the $B_s$ was determined. Compared to running at $\mu = 0.4$, the loss in efficiency at $\mu = 2$ and 4 is respectively 13% and 36%. The deterioration in tracking efficiency due to large occupancies is therefore expected to be small compared to the luminosity increase up to $\mu = 2$. For larger $\mu$ values, the increase in luminosity would be neutralised by the loss in reconstructing multi-body final states.

## 1.4 Consequences for the upgrade strategy

The above would indicate that the present detector could run at luminosities $L \sim 10^{33}$ cm$^{-2}$s$^{-1}$ with $\mu = 2$ if the machine reaches its nominal number of bunches. However, the present detector is limited to a maximum read-out rate of 1.1 MHz. To trigger at an increased event rate requires a substantial change in the LHCb read-out architecture.

The present first level trigger (L0) is implemented in hardware [13]. Trigger selections are

[1]The arrival time of each particle and electronic response may span more than the time interval between consecutive bunches. The simulation takes this into account, also generating interaction several bunches around the bunch of interest.

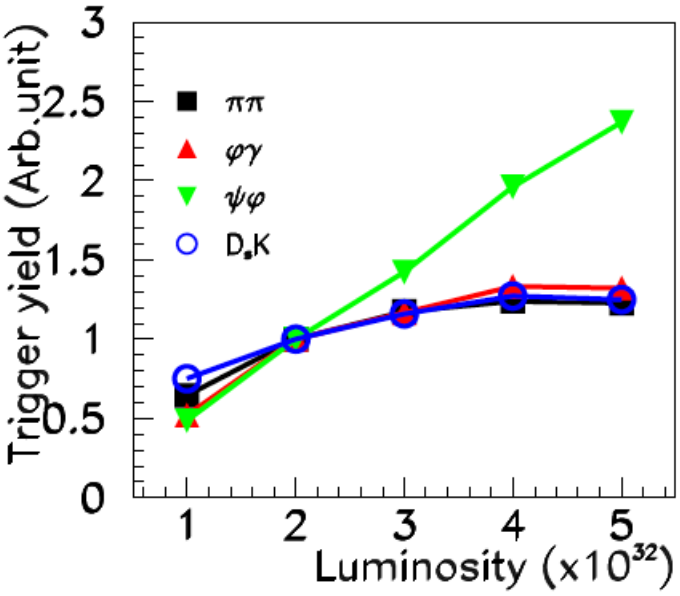


Figure 1.5: The trigger yield for different decays of $B$ mesons. Each point is normalised to the trigger yield expected in nominal conditions at a luminosity of $2 \times 10^{32}$ cm$^{-2}$s$^{-1}$.

made at the 40 MHz beam crossing rate using either the Calorimeters or the Muon System. Criteria are based on the deposit of several GeV of transverse energy, $E_{\rm T}$, by charged hadrons, muons, electrons or photons. While this provides high efficiencies on dimuon events, it typically removes half of the fully hadronic signal decays. In these hadronic decays the $E_{\rm T}$ threshold required to reduce the rate of triggered events to an acceptable level is already a substantial fraction of the $B$ meson mass. Any further increase in the rate requires an increase of this threshold, which then removes a substantial fraction of signal decays. As shown in Fig. 1.5, the trigger yield therefore saturates for hadronic channels with increasing luminosity. While it was shown above that LHCb would be able to run at $L = 10^{33}$ cm$^{-2}$s$^{-1}$, the decrease in L0-efficiencies, and especially the L0-hadron efficiency, would result in an almost constant signal yield, independent of luminosity, for $L > 2$–$3 \times 10^{32}$ cm$^{-2}$s$^{-1}$. Unless the efficiency can be improved by removing the L0 1 MHz limitation and introducing information that is more discriminating than $E_{\rm T}$ earlier in the trigger, the experiment cannot profit from increasing the luminosity.

The most effective way of achieving such a trigger upgrade is to supply the full event information, including whether tracks originate from the displaced vertex that is characteristic of heavy flavour decays, at each level of the trigger. This requires reading out the whole detector at 40 MHz and then analysing each event in a trigger system implemented in software. A detector upgraded in this way would allow the yield of hadronic $B$ decays to be increased by up to a factor of seven for the same LHC machine run-time.

In order to supply displaced vertex information at the first level of the trigger, a tracking system which allows the pattern recognition to be performed quickly is essential. If the tracking system can also improve the efficiency and, in particular, reduce the ghost rate, it may be

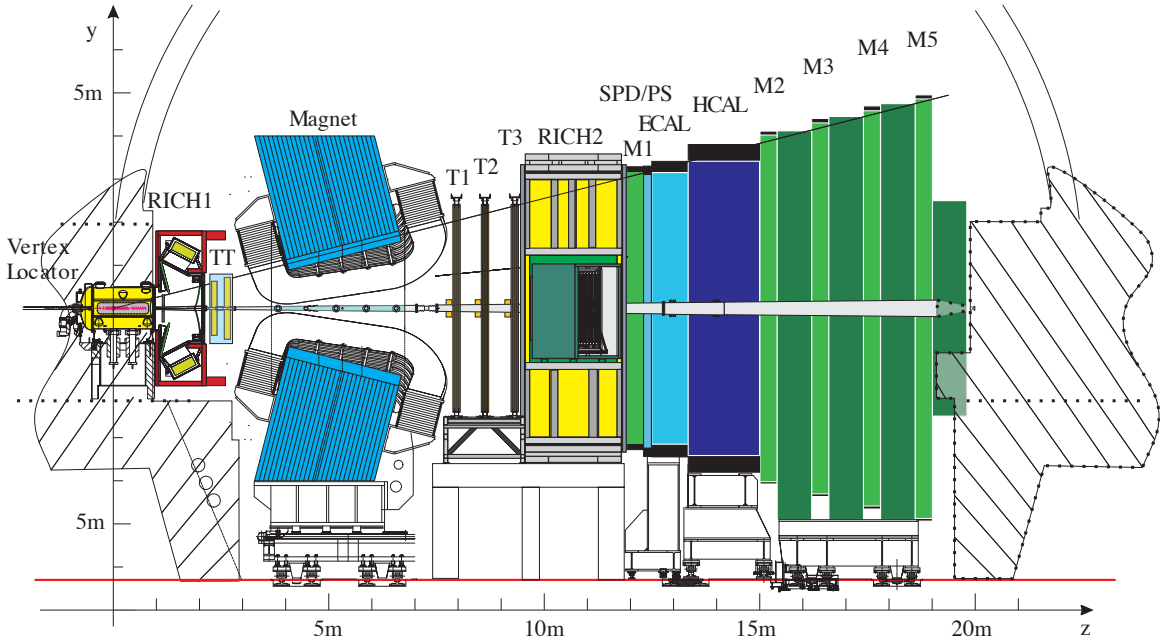


Figure 1.6: Layout of the current LHCb detector.

possible to avoid the efficiency loss for multi-body final states described above which limits the present detector to $\mu = 2$. Running at even higher pile-up would allow further gains in signal yields.

## 1.5 Detector modifications

The current LHCb detector is shown in Fig. 1.6. The detector elements are placed along the beam line of the LHC starting with the Vertex Locator (VELO), a silicon strip device that surrounds the proton-proton interaction region and is positioned with its sensitive area 8 mm from the beam during collisions. It provides precise locations for primary $pp$ interaction vertices, the locations of decays of long-lived particles, and contributes to the measurement of track momenta. Other devices used to measure track momenta comprise a large area silicon strip detector (TT) located in front of a 4 Tm dipole magnet, and a combination of silicon strip detectors (Inner Tracker, IT) and straw drift chambers (Outer Tracker, OT) placed behind. Two ring-imaging Cherenkov (RICH) detectors are used to identify charged hadrons. Further downstream an Electromagnetic Calorimeter (ECAL) is used for photon detection and electron identification, followed by a Hadron Calorimeter (HCAL), and a system consisting of alternating layers of iron and chambers (MWPC and triple-GEM) that distinguishes muons from hadrons (Muon System). The ECAL, HCAL and Muon System provide the capability of first-level hardware triggering.

In this document the next chapter provides a detailed physics case for the LHCb upgrade, and is followed by a chapter describing the detector upgrades. Implementing the 40 MHz read-out for the upgrade will require replacing all the front-end electronics. Apart from this, coping with luminosities of $10^{33}\text{cm}^{-2}\text{s}^{-1}$ does not require substantial rebuilds of the Muon

System, Outer Tracker and calorimeters. For the RICH detectors, the vessels will be reused, but since the front-end electronics is encapsulated within the current photon detectors (HPDs) they will need to be replaced. The VELO sensors will also have to be replaced, due to the increased radiation dose expected in the upgrade. The possibility of equipping it with pixel sensors is under study, as discussed in Section 3.3. Replacement of the silicon tracking stations is also required, since the front-end electronics is attached to the sensors. The possibility of increasing the tracking efficiency by redesigning the stations is under investigation, as presented in Section 3.4.

In addition, owing to the higher occupancies in the upgrade environment, the RICH aerogel radiator and the first muon station (M1) will be removed. The removal of the preshower (PS), and scintillating pad detector (SPD) is also being considered. A new component of the particle identification system based on time-of-flight (TORCH) is proposed to augment the low-momentum particle identification capabilities (see Section 3.5). Upgrades to the calorimetry and MUON systems are described in the subsequent section.

## 1.6 Time-line

LHCb expects to accumulate on the order of 5 $\text{fb}^{-1}$ in the years up to 2017. At that time it is proposed to install the upgrade to allow $\sim 5$ $\text{fb}^{-1}$ to be accumulated each year. This upgrade would not be tied to any luminosity increase of the LHC, as by that time it is expected that $L > 10^{33}\,\text{cm}^{-2}\text{s}^{-1}$ will already be available. The open geometry of the LHCb detector will allow portions of the upgraded detector to be installed in any reasonably long shutdown.

# Chapter 2

# Physics Justification

## Introduction

The LHCb upgrade will pursue important and exciting physics goals in the flavour sector and beyond. The upgrade augments the established strengths of the existing detector, for example the forward acceptance, precise vertexing, and particle identification capabilities, with a flexible software trigger, and the ability to run at a luminosity of $10^{33}\,\mathrm{cm}^{-2}\mathrm{s}^{-1}$, which will enable a very large data sample of $\sim 50\,\mathrm{fb}^{-1}$ to be accumulated. The improvements to the present detector will enable the detector to increase significantly the sensitivity that the experiment can attain in its study of $b$- and $c$-hadron decays, and will make possible high precision measurements and unique studies in many other areas of high energy physics.

In what follows, consideration is given first to the contribution that the upgraded experiment will bring to the field of quark flavour physics. The extremely promising results obtained with first data can already be used to extrapolate to the performance of the future detector. It is argued that measurements in the hadronic flavour sector, i.e. decays of beauty and charm hadrons, have great and wide-ranging sensitivity to New Physics effects. These measurements will be a powerful method both to search for New Physics, and to characterise its nature when found. As such, they constitute an indispensable element of LHC exploitation. The upgrade to the detector proposed in this document is necessary for this programme to proceed throughout the lifetime of the LHC.

The scientific goals of LHCb, however, extend far beyond quark-flavour physics. The upgraded experiment can be regarded as a multi-purpose detector in the forward direction. The unique acceptance, coupled with the flexible trigger, will enable LHCb to make measurements that are either complementary to, or of higher sensitivity than, those which are possible at the LHC general-purpose detectors (ATLAS/CMS) and other facilities. Examples include the search for long-lived exotic particles, and measurements in the electroweak sector such as the determination of the weak mixing angle. A brief survey is therefore made of various opportunities which exist for LHCb in the lepton sector and in non-flavour topics. In most of these areas work is only now beginning, and further study is needed to quantify more precisely the sensitivities that can be achieved. Nevertheless, a clear message emerges as to the richness of the physics possibilities that are open to LHCb beyond the studies of $b$ and $c$ decays.

# 2.1 Quark Flavour Physics

## 2.1.1 Motivation and strategy

The LHCb detector was constructed to study the physics of flavour and its unique capability to probe this sector remains at the core of the physics programme of the upgraded experiment. This is motivated by one of the major unsolved scientific challenges for particle physics, namely the quest to understand the origin of the asymmetry between matter and antimatter in the Universe.

Previous experiments have made a number of measurements of $CP$ violation in the quark sector, and until now all results are compatible with a sole source of asymmetry arising in the Cabibbo-Kobayashi-Maskawa (CKM) quark-mixing matrix [14]. For reviews of the status of the field, see, for example, Refs. [15, 16]. However, it is well known that the Standard Model (SM) $CP$ violation is insufficient to explain the magnitude of the baryon asymmetry of the Universe, and therefore further sources of $CP$ violation must exist. It is possible that these new sources could be found in the lepton sector, or indeed in an extended gauge sector. Nonetheless, the best chance of finding non-standard $CP$ violation effects within the next decade is in the quark sector, due to the high precision that can be achieved with an upgraded LHCb detector exploiting the copious production of charm and beauty hadrons at the LHC.

Flavour observables are also highly sensitive to physics beyond the Standard Model, even in models which do not introduce any new sources of $CP$ violation. The suppression of flavour-changing neutral currents in the SM is one of the most severe constraints for model builders, and effects of virtual particles in rare processes can modify decay rates dramatically from their SM predictions. Historically, such observations resulted in the prediction both of the existence and the properties of the charm quark, as well as the third family (bottom and top quarks) well before colliders reached the energies necessary to produce these particles.

Indeed, there are excellent prospects for major discoveries in the first phase of LHCb operation. If, for example, the true value of the $CP$ violation phase in $B_s$ or $D^0$ oscillations, or that of the decay rate for $B_s \to \mu^+\mu^-$, is substantially altered from the SM prediction, then LHCb measurements will prove the existence of New Physics (NP). Of course, there may also be discoveries of beyond-the-SM physics at ATLAS and CMS. In these scenarios the role of the upgraded LHCb experiment will be to characterise NP, i.e. to understand what is the correct model describing the new phenomena and to measure its parameters. Examples of the impact of measurements from the upgraded LHCb experiment on some illustrative models are given below. In the less favourable scenario that there is no early discovery at the LHC that is inconsistent with the Standard Model, it will be necessary to maximise the possibility of the discovery of New Physics, leaving no stone unturned in the search. The flexible software trigger of the LHCb upgrade will be crucial for this purpose.

To illustrate the impact of the LHCb upgrade beyond the first phase of LHCb operation, we consider some of the key physics analyses discussed in the recent Roadmap document [11]. In each case, the upgraded experiment will provide a significant increase in the physics reach as new regimes of sensitivity are reached, and as the data samples become large enough to study additional decay modes.

| | |
|---|---|
| | **Measurement of mixing-induced $CP$ violation in $B_s \to J/\psi\phi$** |
| *First phase* | Find or rule out large deviations from SM |
| *Upgrade* | Precise measurement of $B_s$ oscillation phase |
| | **Charmless hadronic two-body $B$ decays** |
| *First phase* | Measure $CP$ violation in two-body decays |
| *Upgrade* | Analysis of theoretically clean vector-vector final states |
| | **The tree-level determination of the unitarity triangle angle $\gamma$** |
| *First phase* | Measure with $\sim 4^\circ$ uncertainty to allow for CKM tests |
| *Upgrade* | Achieve $\leq 1^\circ$ precision to match anticipated progress in lattice QCD |
| | **Analysis of the decay $B_s \to \mu^+\mu^-$** |
| *First phase* | Find or rule out large deviations from SM |
| *Upgrade* | Make precision measurement and extend programme to $B^0 \to \mu^+\mu^-$ |
| | **Analysis of the decay $B^0 \to K^{*0}\mu^+\mu^-$** |
| *First phase* | Measure the zero-crossing point of the forward-backward asymmetry |
| *Upgrade* | Exploit the NP sensitivity of the full kinematic distributions |

These measurements are discussed in more detail in the remainder of this section, together with illustrative examples of other important avenues of study, such as the measurement of photon polarisation in exclusive $b \to s\gamma^{(*)}$ decays and the search for $CP$ violation in charm.

In the first phase of the experiment, LHCb will explore areas that (some first measurements by the Tevatron experiments notwithstanding) are virgin territory. Whatever the outcome of this initial exploration, precision measurements of these important quantities will be required. Since the proposed "Super B-factory" experiments cannot compete in a number of key measurements, this can *only* be done with the LHCb upgrade. LHCb has unique potential in the $B_s$ and $b$ baryon sectors, since these particles are not produced in $e^+e^-$ collisions at the $\Upsilon(4S)$ resonance. It will be the only experiment that can perform time-dependent $CP$ violation measurements in the $B_s$ system. Moreover, in exclusive final states composed solely of charged particles, LHCb will accumulate enormous numbers of events, far in excess of what will be available at any other facility. These will allow for super-precise measurements of fundamental quantities such as the $CP$ violating angle $\gamma$, and unchallenged sensitivity to $CP$ violation in charm. A summary of the achievable sensitivities for some key channels is given in Table 2.1, based on the studies presented in [11] and recent updates.

### 2.1.2 Impact on New Physics models

In any scenario, the LHCb upgrade will provide measurements that will be essential to understand the physics landscape that this decade will unveil. In this section we provide some brief examples of the impact of the experiment.

The minimal flavour violation (MFV) hypothesis [17] has been proposed to resolve the tension between the need for physics beyond the SM to manifest at the TeV scale in order to resolve the hierarchy problem, and the apparent absence of effects from new TeV-scale particles in flavour observables (see Refs. [18, 19] for reviews). MFV requires that all sources of flavour- and $CP$-violation in the quark sector have the same pattern as those of the SM, namely the CKM matrix. This can be (albeit sometimes rather unnaturally) satisfied in a range of NP models, including supersymmetry. While such models predict that all measurements of $CP$ violation will be consistent with the SM, large enhancements are possible in rare decays. A

Table 2.1: Sensitivities of the LHCb upgrade to key observables. For each observable the current sensitivity is compared to that expected after LHCb has accumulated 5 fb$^{-1}$ and that which will be achieved with 50 fb$^{-1}$ by the upgraded experiment, all assuming $\sqrt{s} = 14$ TeV. (Note that at the upgraded experiment the yield/fb$^{-1}$ in hadronic $B$ and $D$ decays will be higher on account of the software trigger.)

| Type | Observable | Current precision | LHCb (5 fb$^{-1}$) | Upgrade (50 fb$^{-1}$) | Theory uncertainty |
|---|---|---|---|---|---|
| Gluonic penguin | $S(B_s \to \phi\phi)$ | - | 0.08 | 0.02 | 0.02 |
| | $S(B_s \to K^{*0}\bar{K}^{*0})$ | - | 0.07 | 0.02 | $< 0.02$ |
| | $S(B^0 \to \phi K^0_S)$ | 0.17 | 0.15 | 0.03 | 0.02 |
| $B_s$ mixing | $2\beta_s$ $(B_s \to J/\psi\phi)$ | 0.35 | 0.019 | 0.006 | $\sim 0.003$ |
| Right-handed currents | $S(B_s \to \phi\gamma)$ | - | 0.07 | 0.02 | $< 0.01$ |
| | $\mathcal{A}^{\Delta\Gamma_s}(B_s \to \phi\gamma)$ | - | 0.14 | 0.03 | 0.02 |
| E/W penguin | $A_T^{(2)}(B^0 \to K^{*0}\mu^+\mu^-)$ | - | 0.14 | 0.04 | 0.05 |
| | $s_0\, A_{\rm FB}(B^0 \to K^{*0}\mu^+\mu^-)$ | - | 4% | 1% | 7% |
| Higgs penguin | $\mathcal{B}(B_s \to \mu^+\mu^-)$ | - | 30% | 8% | $< 10\%$ |
| | $\frac{\mathcal{B}(B^0\to\mu^+\mu^-)}{\mathcal{B}(B_s\to\mu^+\mu^-)}$ | - | - | $\sim 35\%$ | $\sim 5\%$ |
| Unitarity triangle angles | $\gamma$ $(B \to D^{(*)}K^{(*)})$ | $\sim 20^\circ$ | $\sim 4^\circ$ | $0.9^\circ$ | negligible |
| | $\gamma$ $(B_s \to D_s K)$ | - | $\sim 7^\circ$ | $1.5^\circ$ | negligible |
| | $\beta$ $(B^0 \to J/\psi\, K^0)$ | $1^\circ$ | $0.5^\circ$ | $0.2^\circ$ | negligible |
| Charm CPV | $A_\Gamma$ | $2.5 \times 10^{-3}$ | $2 \times 10^{-4}$ | $4 \times 10^{-5}$ | - |
| | $A_{CP}^{dir}(KK) - A_{CP}^{dir}(\pi\pi)$ | $4.3 \times 10^{-3}$ | $4 \times 10^{-4}$ | $8 \times 10^{-5}$ | - |

striking example is the branching fraction of the decay $B_s \to \mu^+\mu^-$, which in the CMSSM at large values of $\tan\beta$ (the ratio of Higgs vacuum expectation values) is proportional to $\tan^6\beta$ [20]. Enhancements above the SM prediction of $\mathcal{B}(B_s \to \mu^+\mu^-) = (3.6 \pm 0.3) \times 10^{-9}$ [21] right up to the current experimental upper limit of $5.1 \times 10^{-8}$ [22] are therefore possible.

Although MFV can easily be disproved (for example by any measurement of $CP$ violation that is inconsistent with the SM), it will be difficult to establish for certain if it is an underlying feature of nature. Yet if NP does respect MFV, it will be crucial to know this for sure, since it will provide insight into the underlying physics at very high energies. For example, in supersymmetry MFV is realised if the supersymmetry breaking terms are flavour-blind at the appropriate scale. A proof of the MFV hypothesis can be achieved only by showing that physics beyond the SM exhibits its characteristic flavour-universality pattern. In particular, it is crucial to measure the ratio $\mathcal{B}(B^0 \to \mu^+\mu^-)/\mathcal{B}(B_s \to \mu^+\mu^-)$, since MFV predicts that this is given by its SM value, $|V_{td}/V_{ts}|^2$. Observation of $B^0 \to \mu^+\mu^-$ requires huge statistics and excellent control of backgrounds, and can only be made by the upgraded LHCb experiment.

As an alternative to MFV, we consider a model that has received a lot of attention in the literature recently (see, for example, Refs. [23]), namely the Standard Model extended to four families (SM4). In the quark sector, this model has an extra seven parameters compared to the Standard Model: the masses of the two new quarks ($t'$, $b'$) plus five new quark-mixing parameters, related to the fact that the four-family version of the CKM matrix has nine free

parameters instead of just four as in the SM. These five new quark-mixing parameters can be written as three mixing angles plus two new $CP$-violating phases. The consistency of current flavour measurements with the SM places limits on the sizes of the new mixing angles, while direct searches and electroweak fits constrain the masses of, and the mass difference between, the $t'$ and $b'$ quarks.

In contrast to models with MFV, in SM4 new $CP$-violating phenomena can be expected due to the two new phases. Measuring the underlying parameters of the model becomes a significant challenge due to their strong correlations in most observables. Particularly crucial due to their relatively clean interpretations are the $CP$-violating asymmetries of $D^0$, $B^0$ and $B_s$ oscillations and the phase $\gamma$ [24]. The latter, in particular, can be determined from $B \to DK$ processes with negligible theoretical uncertainty—it yields the SM value of $\gamma$ even in extended models. Only the LHCb upgrade can make the complete set of these measurements with the precision necessary to disentangle the underlying parameters of the model.

As an aside, we note that it is natural to expect that, if there is a fourth family of quarks, the lepton sector will be similarly extended. This can lead to some interesting phenomenology that the LHCb upgrade would be well-placed to explore, as discussed in Section 2.2.1.

### 2.1.3 $CP$ violation

**$CP$ Violation in $B_s$ Oscillations**

One of the primary goals of LHCb is to probe NP in $B_s$ mixing. The golden channel for this analysis is $B_s \to J/\psi\phi$, which is dominated by a $b \to c\bar{c}s$ tree diagram, and therefore is sensitive to the weak phase $\beta_s = \arg\left(-V_{ts}V_{tb}^*/V_{cs}V_{cb}^*\right)$ with little theoretical uncertainty. The measurement proceeds by analysis of the time-dependent and angular decay distributions of $B_s$ mesons. The time-evolution of a $B_s$ meson that is tagged as $\bar{B}_s$ or $B_s$ at time $t = 0$ to a final state $f$ is given by [25]

$$\begin{aligned}
\Gamma_{\bar{B}_s \to f}(t) &= \frac{\mathcal{N}_f e^{-t/\tau(B_s)}}{4\tau(B_s)}\Big[\cosh\left(\frac{\Delta\Gamma_s t}{2}\right) \\
&\qquad + S_f \sin(\Delta m_s t) - C_f \cos(\Delta m_s t) + \mathcal{A}_f^{\Delta\Gamma} \sinh\left(\frac{\Delta\Gamma_s t}{2}\right)\Big], \\
\Gamma_{B_s \to f}(t) &= \frac{\mathcal{N}_f e^{-t/\tau(B_s)}}{4\tau(B_s)}\Big[\cosh\left(\frac{\Delta\Gamma_s t}{2}\right) \\
&\qquad - S_f \sin(\Delta m_s t) + C_f \cos(\Delta m_s t) + \mathcal{A}_f^{\Delta\Gamma} \sinh\left(\frac{\Delta\Gamma_s t}{2}\right)\Big], \qquad (2.1)
\end{aligned}$$

where

$$S_f = \frac{2\,\mathrm{Im}(\lambda_f)}{1+|\lambda_f|^2}, \quad C_f = \frac{1-|\lambda_f|^2}{1+|\lambda_f|^2}, \quad \mathcal{A}_f^{\Delta\Gamma} = -\frac{2\,\mathrm{Re}(\lambda_f)}{1+|\lambda_f|^2}, \quad \text{and} \quad \lambda_f = \frac{q}{p}\frac{\bar{A}_f}{A_f}.$$

Note that $(S_f)^2 + (C_f)^2 + \left(\mathcal{A}_f^{\Delta\Gamma}\right)^2 = 1$ by definition, and that in contrast to the $CP$-violating asymmetry parameters $S_f$ and $C_f$, the parameter $\mathcal{A}_f^{\Delta\Gamma}$ appears with the same sign in both $\bar{B}_s$ and $B_s$ decay time distributions, and can therefore be determined from untagged analysis.

The parameters $\bar{A}_f$ and $A_f$ are the complex amplitudes for the decay of $\bar{B}_s$ and $B_s$ to the final state $f$, respectively. For a $CP$ eigenstate decay, $\lambda_f$ takes a single value (so that if,

for a decay to a CP-even eigenstate, the $b \to c\bar{c}s$ tree diagram is dominant, $S_f = \sin(2\beta_s)$ and $\mathcal{A}_f^{\Delta\Gamma} = -\cos(2\beta_f))$ but for a vector-vector final state $\lambda_f$ is written as a function of the contributing helicity amplitudes, appropriately weighted for each particular point in phase space, giving a more complicated dependence on $\beta_s$ [25]. The parameters $q$ and $p$ describe the eigenstates of the effective weak Hamiltonian of the $B_s$–$\bar{B}_s$ system (see Eq. 2.2 below). The constant $\mathcal{N}_f$ is a normalisation factor.

In the Standard Model, the value of $\beta_s$ is constrained from global fits to the CKM matrix to be close to zero (see, for example, Refs. [5,6]), $2\beta_s = -2\eta\lambda^2 = -0.0363 \pm 0.0017\,\text{rad}$, where $\eta$ and $\lambda$ are the Wolfenstein parameters [26] of the CKM matrix. Although first measurements of $\beta_s$ have been made by CDF [7] and D0 [8], the results to date do not provide a very significant constraint.

The signals of $J/\psi K^{(*)}$ and $J/\psi\phi$ decays seen in the early LHCb data shown in Fig. 2.1 are in line with the expected yields. Moreover, it has already been possible, and using hadronic final states such as $B_s \to D_s\pi$, to resolve the very rapid $B_s$ oscillations and measure $\Delta m_s$, the parameter which determines the mixing frequency. The likelihood scan as a function of $\Delta m_s$ is shown in Fig. 2.2. A clear minimum is seen, and the preliminary analysis yields $\Delta m_s = 17.63 \pm 0.11\,(\text{stat}) \pm 0.04\ \text{ps}^{-1}$ [27], in good agreement with the value from the Tevatron of $17.77 \pm 0.12\ \text{ps}^{-1}$ [30].

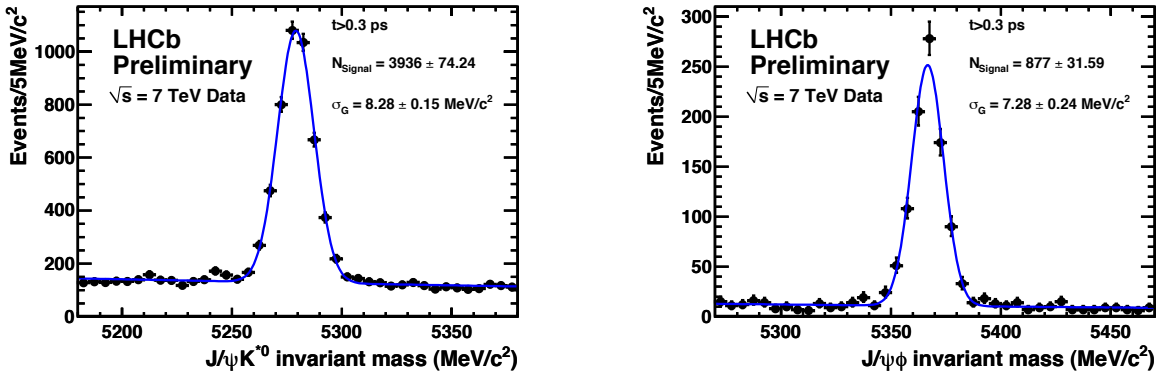


Figure 2.1: Signals for (left) $B^0 \to J/\psi K^{*0}$ and (right) $B_s \to J/\psi\phi$ seen in $\sim 34\ \text{pb}^{-1}$ of LHCb data accumulated in 2010.

With $\sim 337\ \text{pb}^{-1}$ of LHCb data accumulated in 2011, a preliminary value of $\phi_s = 0.13 \pm 0.18\,(\text{stat}) \pm 0.07$ rad is obtained using the decay $B_s \to J/\psi\phi$ [29], surpassing the sensitivities obtained as other experiments. The result is displayed in the $\phi_s^{J/\psi\phi} - \Delta\Gamma$ plane in Fig. 2.3.

Given these encouraging first results from data, and from the results of simulation sensitivity studies [11], we can be confident that with $5\ \text{fb}^{-1}$ accumulated during the first phase of LHCb, $\beta_s$ will be determined with a statistical precision comparable to the central value of the Standard Model prediction [11]. This accuracy is good enough to establish a New Physics effect if it is only three times larger than the SM.

If no anomalous effect is seen, it will be necessary to improve the precision to be able to observe $CP$ violation at the SM level. In this case, and also if anomalies are found, it will be necessary to control both experimental (systematic) and theoretical uncertainties. These challenges can be tackled in the upgraded experiment using several complementary approaches.

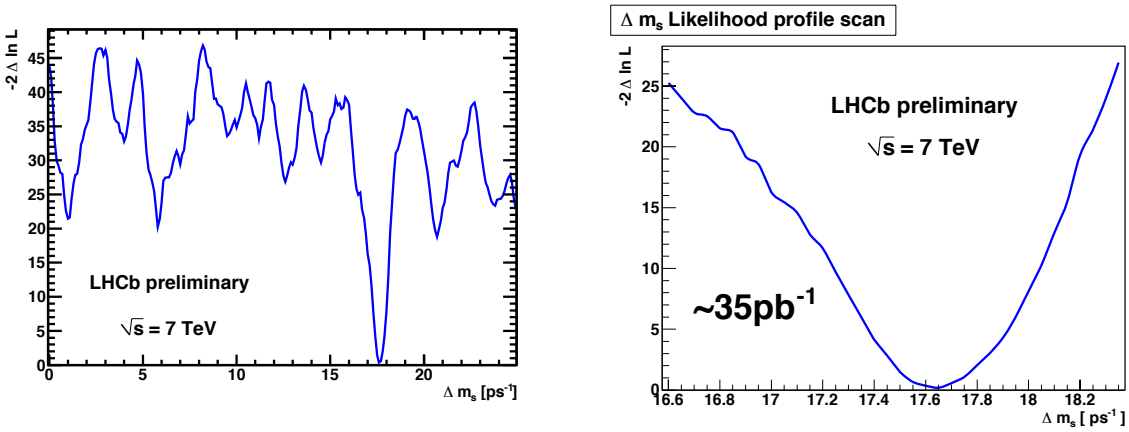


Figure 2.2: LHCb preliminary likelihood profile scans for $\Delta m_s$ for a wide $\Delta m_s$ range (left) and a narrower one (right). Only statistical uncertainties are considered here [27].

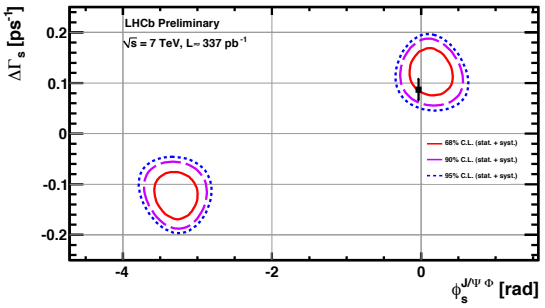


Figure 2.3: 2D likelihood confidence regions in the $\phi_s^{J/\psi\phi} - \Delta\Gamma$ plane. The black square ss corresponds to the theoretical predicted Standard Model value [28].

- The measurement using $J/\psi\phi$ decays can suffer systematic uncertainties from acceptance effects since an angular analysis of the vector-vector final state is required:
  $\hookrightarrow$ $\beta_s$ can be measured using $B_s$ decays via $b \to c\bar{c}s$ transitions to pure $CP$ eigenstates such as $D_s^+ D_s^-$ and $J/\psi f_0(980)$, which has recently been observed for the first time by LHCb, as shown in Fig. 2.4 [31]. Using the $B_s \to J/\psi f_0(980)$ decay in $\sim 378$ pb$^{-1}$ of LHCb data accumulated in 2011, a preliminary value of $\phi_s = -0.44 \pm 0.44\,(\text{stat}) \pm 0.02$ rad could already be obtained [32].

- Contributions from S-wave $K^+K^-$ under the $\phi$ peak can bias the measurement if not properly accounted for [33]:
  $\hookrightarrow$ the additional amplitudes can be included in the fit, which will remove the bias [34].

- Uncertainties arise in the SM prediction due to suppressed (penguin) contributions to the decay amplitude:
  $\hookrightarrow$ the SM uncertainties can be bounded from data using the $B_s \to J/\psi K^{(*)0}$ decays [35, 36]; $\beta_s$ can be measured in the penguin-free $B_s \to D^0\phi$ channel [37].

The upgraded LHCb experiment will also allow for a significant improvement in the knowledge of the $CP$ violating phase in $B^0$ oscillations, $\beta$. While the measurement of $\sin 2\beta$ using

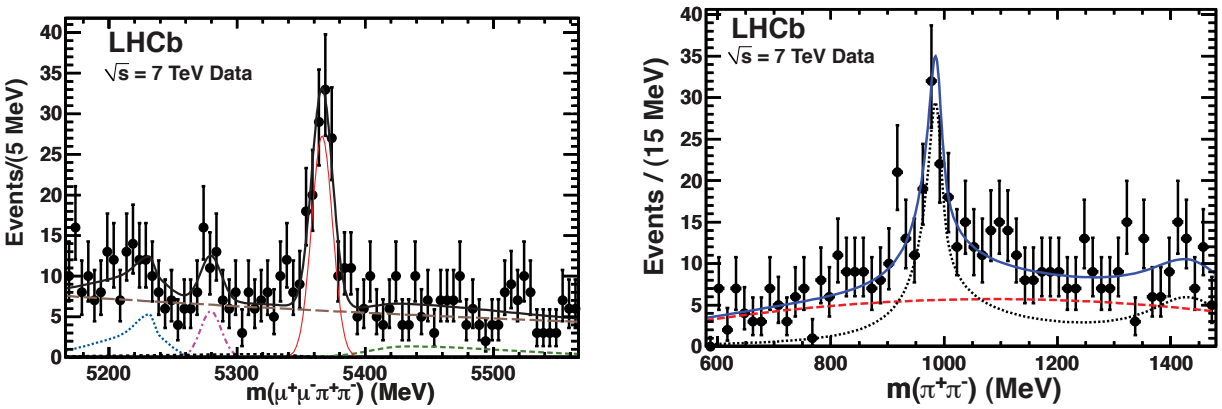


Figure 2.4: Signal for $B_s \to J/\psi f_0(980)$ seen in $\sim 33$ pb$^{-1}$ of LHCb data accumulated in 2010 [31]. (Left) $B_s$ candidate invariant mass distribution for candidates with $|m(\pi^+\pi^-) - 980 \text{ MeV}| < 90$ MeV; (right) $m(\pi^+\pi^-)$ distribution for candidates with $|m(J/\psi\pi^+\pi^-) - 5366 \text{ MeV}| < 30$ MeV.

the decay $B^0 \to J/\psi K^0_S$ will be a calibration measurement in the early period of LHCb data taking, the very high statistics of the upgraded experiment will allow for a significantly better sensitivity than the present world average. Similar strategies to those discussed above for the $B_s$ oscillation phase can be used to control theoretical uncertainties.

A complementary approach to search for New Physics effects in $B_s$ oscillations is through the measurement of $CP$ violation that arises in the mixing amplitude itself (as opposed to the effects discussed above, which correspond to $CP$ violation in the interference of mixing and decay). The parameters $p$ and $q$ introduced in Eq. 2.1 are defined by writing the mass eigenstates of the effective weak Hamiltonian [25]

$$|B_L\rangle = p\,|B_s\rangle + q\,\left|\bar{B}_s\right\rangle \qquad |B_H\rangle = p\,|B_s\rangle - q\,\left|\bar{B}_s\right\rangle \tag{2.2}$$

where $|p|^2 + |q|^2 = 1$. $CP$ violation in mixing occurs when $|q/p| \neq 1$, and a $CP$ violation parameter can be defined in analogy with the kaon system as $\varepsilon_{B_s} = (p-q)/(p+q)$. This can be measured using flavour-specific decays where the quantity determined is the so-called flavour-specific asymmetry, $A_{\rm fs}(B_s)$. Inclusive semileptonic decays provide a convenient high-statistics sample with which to determine this quantity,

$$A_{\rm fs}(B_s) = \frac{\Gamma\left(B^0_s\bar{B}^0_s \to l^-l^-X\right) - \Gamma\left(B^0_s\bar{B}^0_s \to l^+l^+X\right)}{\Gamma\left(B^0_s\bar{B}^0_s \to l^-l^-X\right) + \Gamma\left(B^0_s\bar{B}^0_s \to l^+l^+X\right)} = \frac{|p/q|^2 - |q/p|^2}{|p/q|^2 + |q/p|^2} \approx \frac{4\,\mathrm{Re}\,(\varepsilon_{B_s})}{1 + |\varepsilon_{B_s}|^2}\,. \tag{2.3}$$

The SM prediction is $A_{\rm fs}(B_s) = (2.06 \pm 0.57) \times 10^{-5}$ [38], and hence any asymmetry larger than $\sim 10^{-4}$ could only be a consequence of NP.

If the inclusive approach is applied in a hadronic environment, the quantity measured is a linear combination of the flavour-specific asymmetries in $B^0$ and $B_s$ decays. This approach has recently been used by the D0 collaboration [9, 10], with the result

$$A^b_{\rm sl} = (0.506 \pm 0.043) \times A_{\rm fs}(B^0) + (0.494 \pm 0.043) \times A_{\rm fs}(B_s) \tag{2.4}$$

$$= -0.00957 \pm 0.00251\,(\text{stat.}) \pm 0.00146\,(\text{syst.})\,, \tag{2.5}$$

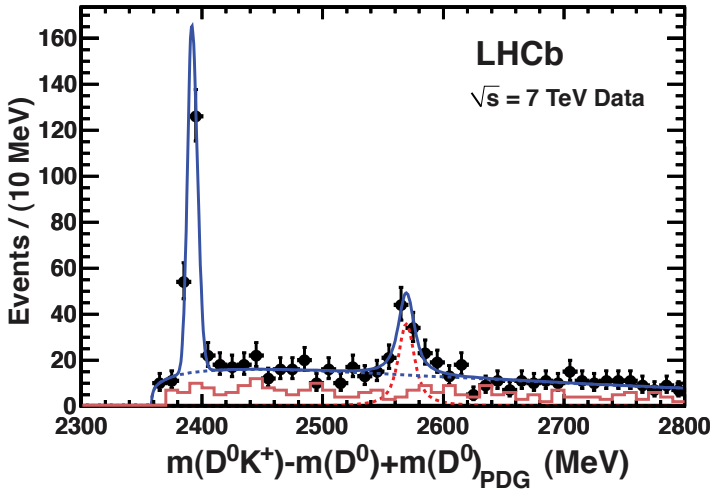


Figure 2.5: Signal for $B_s \to D_{s2}^{*+}\mu^-\nu X$ seen in $\sim 20$ pb$^{-1}$ of LHCb data accumulated in 2010 [39].

which is 3.2 standard deviations from the Standard Model prediction (the SM gives $A_{\rm fs}(B^0) = \left(-4.8\,^{+1.0}_{-1.2}\right) \times 10^{-4}$ [38], so that $A^b_{\rm sl}({\rm SM}) = \left(-2.3\,^{+0.5}_{-0.6}\right) \times 10^{-4}$ [9]).

One urgent goal of the first phase of LHCb is to confirm or rule out this anomaly. Large yields of semileptonic decays have already been recorded and have been used to measure the $b\bar{b}$ production cross-section [12] and to make the first observation of the decay $B_s \to D_{s2}^{*+}\mu^-\nu X$ [39], shown in Fig. 2.5. Due to the high precision required, it is necessary to use methods with intrinsically low levels of systematic uncertainty. The favoured approach in early data taking is to examine the difference between the $B^0$ and $B_s$ flavour-specific asymmetries, identifying $B^0$ and $B_s$ by their decays to $D^-\mu^+X$ and $D_s^-\mu^+X$ respectively, using the identical final state $K^+K^-\pi^-$ for both $D^-$ and $D_s^-$ decays, thereby suppressing biases from any detector asymmetries. A very precise measurement is possible with 5 fb$^{-1}$ [40, 41].

If NP is found in this measurement, it will be necessary to perform separate measurements of $A_{\rm fs}(B^0)$ and $A_{\rm fs}(B_s)$, rather than their combination, to isolate the origin of the effect. While more precise measurements of $A_{\rm fs}(B^0)$ could potentially be made at future $e^+e^-$ B-factories, competitive measurements of the $B_s$ system can only be made at LHCb. Here it will be difficult to use semileptonic decays, since the systematic uncertainty due to intrinsic detector asymmetry will be hard to control. However, the hadronic decay $B_s \to D_s^-\pi^+$ is flavour-specific, and gives a symmetric final state when the $D_s^- \to K^+K^-\pi^-$ decay is used [41]. This analysis will require both very large statistics and a flexible trigger with high efficiency on hadronic decay modes, and therefore can only be carried out at the upgraded LHCb experiment.

As an aside, we mention that among the broad physics programme that can be achieved using semileptonic decays, the upgraded LHCb experiment has promising sensitivity to the decays $B \to D^{(*)}\tau\nu$. The rates of these decays are sensitive to New Physics in two-Higgs-doublet models, including supersymmetry, since tree-level diagrams involving charged Higgs bosons can interfere with the $W$-mediated SM amplitude [42]. The $B \to D^{(*)}\tau\nu$ decays hence probe the same physics as the $e^+e^-$ B-factory golden channel $B^+ \to \tau^+\nu$, but in addition allow for the study of kinematical observables that provide further NP sensitivity [43]. The signature of $B \to D^{(*)}\tau\nu$ decays at LHCb is a three-prong $\tau$ decay together with a $D^{(*)}$ meson, both displaced from a $B$ vertex that is itself displaced from the primary vertex. The decay has a

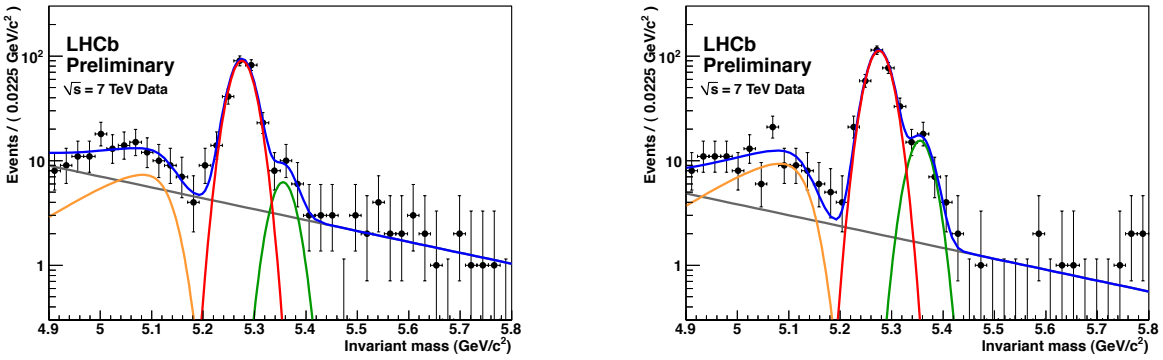


Figure 2.6: Signals for (left) $B_{(s)} \to K^-\pi^+$ and (right) $B_{(s)} \to K^+\pi^-$ seen in $\sim 35$ pb$^{-1}$ of LHCb data accumulated in 2010. Signals for both $B^0$ and $B_s$ decays are visible at the expected levels, and the uncorrected $CP$ asymmetries are consistent with previous measurements [45].

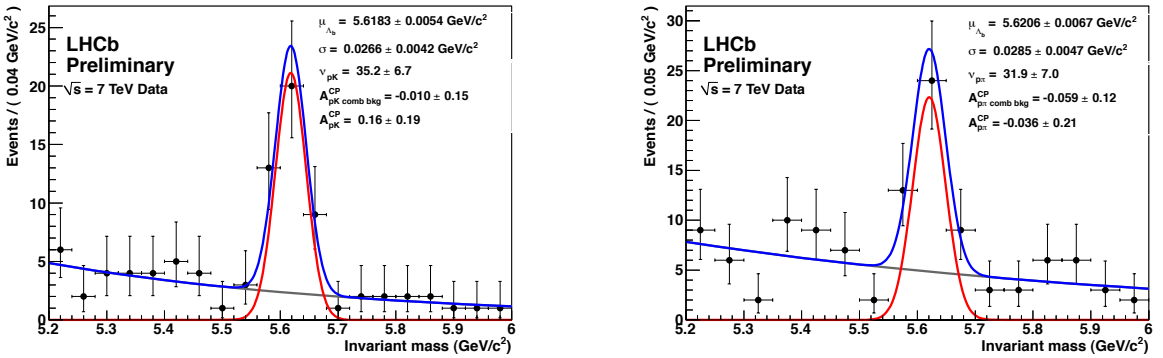


Figure 2.7: Signals for (left) $\Lambda_b \to pK^-$ and (right) $\Lambda_b \to p\pi^-$ (both including charge conjugate modes) seen in $\sim 35$ pb$^{-1}$ of LHCb data accumulated in 2010.

large branching fraction, so very large statistics are in principle available. However, owing to the high multiplicity of the final state, the efficiency for the decay to pass a transverse energy threshold in the trigger is suppressed. This analysis will therefore benefit significantly from the flexible trigger strategy of the LHCb upgrade.

### $CP$ violation in charmless hadronic decays

Charmless hadronic $B$ decays are in principle highly sensitive to NP, since they proceed through rare decay topologies such as penguin diagrams. However, it is an experimental and theoretical challenge to control SM uncertainties to the precision necessary. In the first phase of LHCb, the emphasis is on decays to two charged particles, where clear signals have already been observed [44], as shown in Figs. 2.6 and 2.7. In early data, we expect to make the world's first observations of direct $CP$ violation in $B_s$ and $\Lambda_b$ decays, and to measure time-dependent $CP$ violation in $B_s \to K^+K^-$ decays, which is sensitive to NP. We also expect to observe many new interesting decay channels, such as $B_s \to K^{*0}\bar{K}^{*0}$.

In the upgraded experiment, it will be possible to measure time-dependent $CP$ violation in channels that have only recently been discovered, and even in some that have not yet been

observed. In particularly, the penguin-dominated decays $B_s \to \phi\phi$ and $B_s \to K^{*0}\bar{K}^{*0}$ are particularly sensitive to NP [46]. For the former, the SM prediction for the time-dependent $CP$ violation is very close to zero due to a cancellation of the $B_s$ mixing and decay phases [47]. A SM calculation using QCD factorisation gives a theoretical upper limit of a 2% effect [48]. After collecting 5 fb$^{-1}$ of data with the LHCb experiment, the statistical sensitivity to $CP$ violation in $B_s \to \phi\phi$ is expected to be about 0.08 [49]. The lifetime resolution and acceptance, the angular acceptance, the $B_s$ lifetime and mass differences and the background model will contribute to a total systematic error of about 0.01. Therefore the precision will be at about the same level as achieved by the B-factories for the related modes $B^0 \to \phi K_S$ and $B^0 \to \eta' K_S$, and more statistics will be necessary for further improvement.

The LHCb upgrade will substantially improve the measurement of $CP$ violation in $B_s \to \phi\phi$, since this a hadronic mode which will benefit maximally from the detached vertex trigger. To reach the highest precision it will be necessary to remove the possible S-wave contributions from non-resonant $B_s \to \phi K^+K^-$ and $B_s \to \phi f_0$ decays [33]. Studies have shown that these can be incorporated into the analysis without causing a bias, albeit with an increase in statistical error of less than 15% [34]. With 50 fb$^{-1}$ of data accumulated with the upgraded experiment, a sensitivity of a few percent, comparable to current estimates of the theoretical uncertainty, is achievable.

The decay $B_s \to K^{*0}\bar{K}^{*0}$ has similar phenomenology to $B_s \to \phi\phi$, and the experimental sensitivities that can be reached in the two cases are also comparable. The advantage of this mode is that the SM contribution can be determined from data in a model-independent analysis that uses information extracted from the related $B^0 \to K^{*0}\bar{K}^{*0}$ decays [50].

The polarisation of the decays $B_s \to \phi\phi$ and $B_s \to K^{*0}\bar{K}^{*0}$ is also of great topical interest, due to the so-called "polarisation puzzle", i.e. the unexpectedly large transverse polarisation observed in $B \to \phi K^*$ and $B \to \rho K^*$ decays (see Ref. [51] for reviews). The polarisation of $B_s$ decays to charmless vector-vector final states can be measured to high precision since the analysis does not require flavour-tagging.

The LHCb upgrade will also improve the precision of several interesting measurements involving $\phi$ mesons, such as $B^0 \to \phi K^0_S$ and $B^0 \to \phi K^{*0}$. The CP violating asymmetry in $\phi K^0_S$ can be measured to an accuracy of 0.03 and is expected to be similar to the theoretical uncertainty.

The LHCb upgrade will also be uniquely capable of making the first detailed analyses of multibody decays of the $B_s$ meson, such as $B_s \to K_S\pi^+\pi^-$ and $B_s \to K_S K^\pm\pi^\mp$. Together with the related $B^0$ and $B^+$ channels, analyses of the Dalitz plot distributions provide several exciting prospects for NP searches [52].

**Measurement of the CKM Unitarity Triangle angle $\gamma$**

Searches for New Physics in $CP$ violation effects require precise measurements of Standard Model benchmarks to compare against. Key to this programme is the measurement of the CKM Unitarity Triangle angle $\gamma$, which can be determined with negligible theoretical uncertainty using $B \to DK$ decays such as $B^+ \to DK^+$ [53], $B^0 \to DK^{*0}$ [54] and $B_s \to D_s^\mp K^\pm$ [55].

At present, $\gamma$ is the least well-determined of the three angles of the Unitarity Triangle, and does not provide any significant constraint in global fits fits to the CKM matrix carried out by groups such as CKMfitter [5] and UTfit [6]. This situation will change when results become available from LHCb.

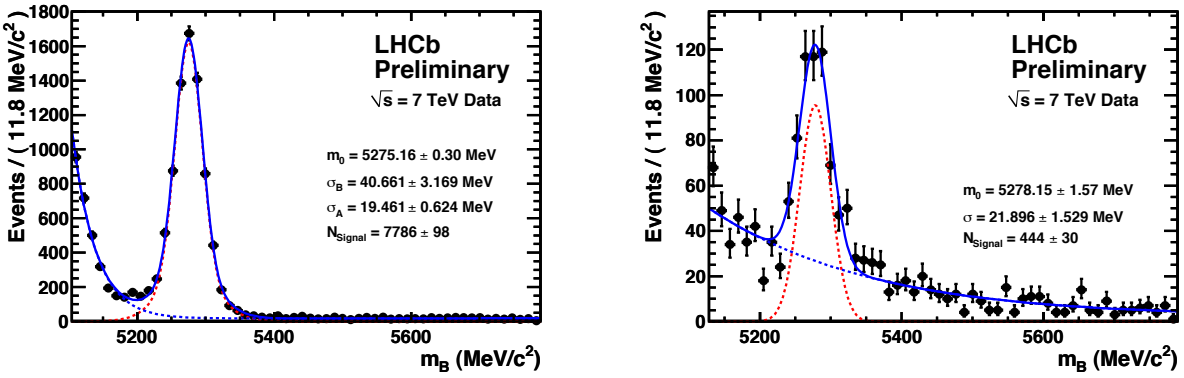


Figure 2.8: Signals for (left) $B^+ \to \bar{D}^0\pi^+$ and (right) $B^+ \to \bar{D}^0 K^+$ seen in $\sim 34$ pb$^{-1}$ of LHCb data accumulated in 2010. In both cases the $\bar{D}^0 \to K^-\pi^+$ decay is used.

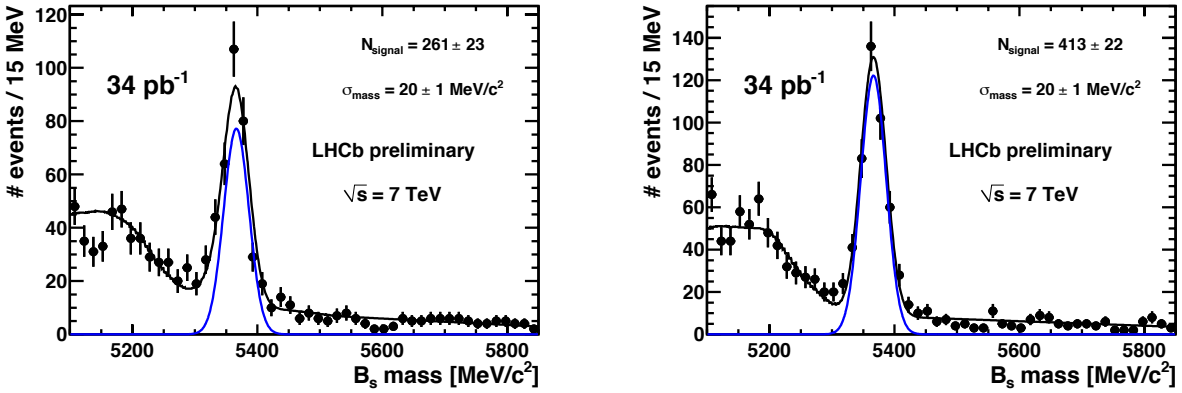


Figure 2.9: Signals for $B_s \to D_s\pi$ with (left) $D_s \to K^*K$ and (right) $D_s \to \phi\pi$ seen in $\sim 34$ pb$^{-1}$ of LHCb data accumulated in 2010.

The signals of $B \to D\pi$ and $B \to DK$ decays already seen by LHCb, shown in Figs. 2.8 and 2.9, illustrate the impact on $\gamma$ that LHCb will make with early data. By combining $\gamma$ measurements from $B \to DK$ and $B_s \to D_s^{\mp}K^{\pm}$, a sensitivity of 3° is expected with 5 fb$^{-1}$. However, precision at the level of one degree or below is necessary to avoid limiting the sensitivity of the global CKM fits to New Physics. Specifically, the indirect constraint on $\gamma$ from the magnitude of the CKM matrix element $V_{ub}$ and the ratio of mass-differences in the neutral $B$ systems, $\Delta m_d/\Delta m_s$, is expected to reach sub-percent accuracy as more advanced lattice calculations become available [56]. This motivates a concerted effort to provide the best possible measurement of $\gamma$.

Only the LHCb upgrade will provide the huge statistics needed to reach the precision that is necessary to remove the Standard Model uncertainty in New Physics searches. Indeed, the measurement of $\gamma$ is ideally suited for LHCb, since it is based largely on analyses (i) that do not require flavour-tagging, and (ii) that exploit LHCb's unique capability to trigger on fully hadronic decay modes. Due to this second reason, the measurement will benefit greatly from the improved trigger strategy of the upgraded experiment. With 50 fb$^{-1}$, $\gamma$ will be determined to better than 1° precision. This will allow to test the consistency of the SM at the percent level.

Moreover, as discussed in Section 2.1.2, once new sources of $CP$ violation are established the measurement of $\gamma$ will be particularly important to disentangle the parameters of the underlying model.

### 2.1.4 Rare decays

**Measurement of $B_s \to \mu^+\mu^-$ and $B^0 \to \mu^+\mu^-$**

One area where the impact of the increased statistical power of the upgraded LHCb experiment is profound is in rare decays. There are several key modes that offer large discovery potential. One of the most interesting is the very rare decay $B_s \to \mu^+\mu^-$. As discussed in Section 2.1.2, this flavour-changing neutral current is heavily suppressed in the SM, and is highly sensitive to New Physics [57]. In particular, in the CMSSM at large $\tan\beta$, the branching fraction $\mathcal{B}(B_s \to \mu^+\mu^-)$ increases as $\tan^6\beta$, where $\tan\beta$ is the ratio of Higgs vacuum expectation values, and depends on the gaugino mass, $m_{1/2}$ and the trilinear soft supersymmetry-breaking parameter $A_0$. The predictions of Ellis *et al.* [58] are shown in Fig. 2.10. The measurement of this branching fraction provides one of the strongest constraints on the parameters of this model at high $\tan\beta$.

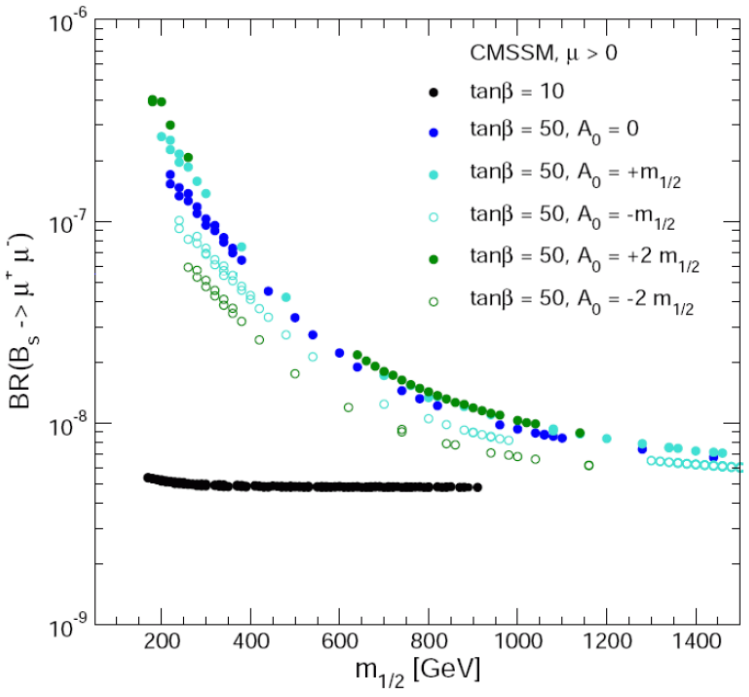


Figure 2.10: Predictions for $\mathcal{B}(B_s \to \mu^+\mu^-)$ as a function of the gaugino mass $m_{1/2}$ for selected values of $\tan\beta$ and the $A_0$ mass. From Ref. [58].

LHCb has reported a search for $B_s \to \mu^+\mu^-$ using about 40 fb$^{-1}$ collected in 2010 [59]. No signal is found, and an upper limit is set at the 90% C.L. of $43 \times 10^{-9}$. This is already very similar to the corresponding limits placed by the Tevatron experiments, which are $36 \times 10^{-9}$ [60] and $42 \times 10^{-9}$ [61], obtained by CDF and D0 with 3.7 fb$^{-1}$ and 6.1 fb$^{-1}$ respectively.

The sensitivity of the first LHCb result agrees with the expectations from the Monte Carlo, and gives confidence for the future of this search over the coming years. The discovery potential

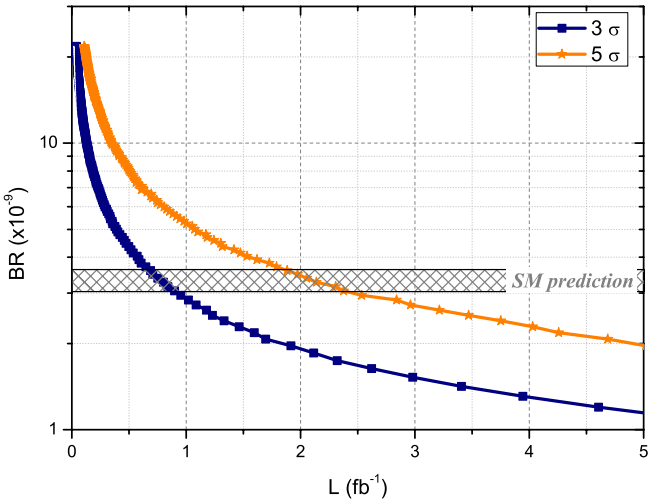


Figure 2.11: Discovery potential of LHCb to $\mathcal{B}(B_s \to \mu^+\mu^-)$ as a function of integrated luminosity for 14 TeV centre-of-mass energy collisions. The upper (lower) curve shows the data sample necessary to discover the decay with 5 (3) $\sigma$ significance.

of LHCb is shown in Fig. 2.11 as a function of integrated luminosity. The figure is made assuming a centre-of-mass energy of 14 TeV.

A preliminary result is obtained with $\sim 300$ pb$^{-1}$ of LHCb data accumulated in 2011 [62]

$$BR(B_s \to \mu\mu) < 1.6 \times 10^{-8}\ 95\%\ CL\,, \tag{2.6}$$

$$BR(B_d \to \mu\mu) < 5.1 \times 10^{-9}\ 95\%\ CL\,. \tag{2.7}$$

Although the sensitivity of the Tevatron experiments has been surpassed, a $5\,\sigma$ discovery will require several years of operation if $\mathcal{B}(B_s \to \mu^+\mu^-)$ is at the SM level, or below. (it is also worth drawing attention to the possibility that in several NP models, in particular those with a Higgs singlet, the branching ratio may indeed be *suppressed* with respect to the SM value [63].)

Whether or not the decay is observed in early LHC data, further improvement will be necessary in the knowledge of its branching fraction. It is important to note that the measurement is expected to be statistically limited. Until recently the knowledge of the ratio of fragmentation fractions, $f_s/f_d$, was thought to provide a limiting factor. However, LHCb has already measured this ratio with semileptonic decays to 10% accuracy [64], and further improvement will occur. Alternative methods to measure $f_s/f_d$ using hadronic decays have also been proposed [65].

With a 50 fb$^{-1}$ data sample the upgraded LHCb experiment would be able to measure the branching ratio $\mathcal{B}(B_s \to \mu^+\mu^-)$ to about 8% precision if it is at the SM level. This will provide unique insights into the flavour properties of NP, and will put very stringent constraints on SUSY models in the large $\tan\beta$ regime. In the ideal scenario that SUSY particles are discovered at ATLAS and CMS, the combination of their results with those from the LHCb upgrade will allow the best constraints on the parameter space.

As soon as $B_s \to \mu^+\mu^-$ is observed for the first time, attention will turn to its sister channel, $B^0 \to \mu^+\mu^-$. As discussed in Section 2.1.2, the correlation between the branching fractions

of these two channels is extremely useful to distinguish between different NP models, and is essential to confirm or rule out the MFV hypothesis [66]. The $B^0$ decay is both much rarer than the $B_s$ decay, and suffers from a larger background from pion misidentification and decay-in-flight, since the branching fraction for $B^0 \to \pi^+\pi^-$ ($5 \times 10^{-6}$ [45]) is much larger than that for $B_s \to \pi^+\pi^-$ ($< 1.2 \times 10^{-6}$ [67]). Therefore the full statistics of the upgraded LHCb experiment, together with excellent control of this background, will be necessary to measure the $B^0 \to \mu^+\mu^-$ decay.

**Analysis of $B^0 \to K^{*0}\mu^+\mu^-$ and related decays**

Exclusive decays of the type $H_b \to H_s\mu^+\mu^-$, where $H_b$ is a $b$-flavoured hadron and $H_s$ is a hadronic system containing an $s$ quark produced in a $b \to s$ flavour-changing neutral current transition as well as the spectator quark(s) from $H_b$, have a high sensitivity to New Physics. Many of these can be reconstructed in large quantities at LHCb: the archetypal channel in this category is $B^0 \to K^{*0}\mu^+\mu^-$, but other decays such as $B^+ \to K^+\mu^+\mu^-$, $B^+ \to K_1^+\mu^+\mu^-$, $B^0 \to K_2^{*0}\mu^+\mu^-$, $B_s \to \phi\mu^+\mu^-$ and $\Lambda_b \to \Lambda^{(*)}\mu^+\mu^-$ will be available in large quantities at the upgraded LHCb experiment, and provide complementary New Physics sensitivity.

One of the characteristic features of the $B^0 \to K^{*0}\mu^+\mu^-$ decay is the forward-backward asymmetry in the angular distribution of the muons in the dimuon rest-frame (relative to the $B^0$ direction) as a function of the dimuon invariant mass, $q^2$. This asymmetry arises as a consequence of interference between the contributing electroweak diagrams, and can be expressed in terms of the Wilson coefficients $C_{7\gamma}$, $C_9$ and $C_{10}$ (see Ref. [4] for a review). Since the relative amplitudes of the interfering diagrams vary as a function of $q^2$, there is a point at which the forward-backward asymmetry crosses zero, usually denoted $q^2 = s_0$. Due to a cancellation of hadronic uncertainties, the value of $s_0$ is cleanly predicted in the SM to be $s_0 = \left(4.36\,^{+0.36}_{-0.33}\right)$ GeV$^2$ [68]. First measurements of the differential distributions have been made by the B-factories and CDF, with results providing an exciting hint of a deviation from the SM prediction [69].

One of the main objectives of the first phase of LHCb data taking is a precise measurement of the forward-backward asymmetry in $B^0 \to K^{*0}\mu^+\mu^-$ decays. LHCb expects to collect 2100 $B^0 \to K^{*0}\mu^+\mu^-$ decays per 1 fb$^{-1}$ at $\sqrt{s} = 14$ TeV, allowing $s_0$ to be measured with precision comparable to the theory error after a few years of data-taking [11]. If large NP effects are present, as hinted at by the current measurements, LHCb will measure a deviation from the SM prediction with high significance. Whether or not NP effects manifest themselves in the early data, it will be necessary to perform higher statistics studies in order to exploit the full sensitivity of these decays. The results of an angular analysis of this process using $\sim 309$ pb$^{-1}$ of LHCb data accumulated in 2011 is shown in Fig. 2.12, and is the most sensitive measurement of the forward-backward asymmetry [70].

The $B^0 \to K^{*0}\mu^+\mu^-$ decay provides extremely rich phenomenology due to the many different kinematic observables that can be studied. In addition to the forward-backward asymmetry, one particularly interesting observable is the transversity asymmetry $A_T^{(2)}$ that can distinguish between different New Physics models [72, 73]. $A_T^{(2)}$ is highly sensitive to new right-handed currents to which the forward-backward asymmetry is blind. In the theoretically favoured region, 1 GeV$^2$ $< q^2 <$ 6 GeV$^2$, the resolution in $A_T^{(2)}$ is estimated at 0.14 with 5 fb$^{-1}$ of integrated luminosity [73]. This is illustrated in Fig. 2.13 where we show $A_T^{(2)}$ versus $q^2$ for the SM and a NP model as well as the experimental sensitivity. It is clear that a larger data

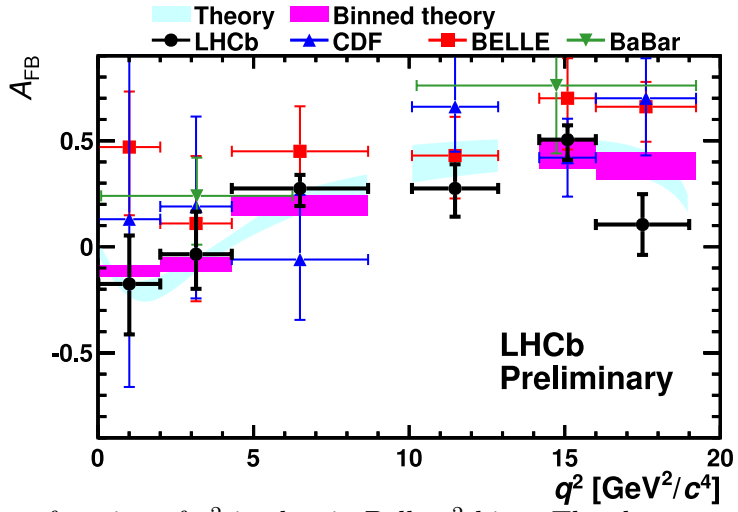


Figure 2.12: $A_{FB}$ as a function of $q^2$ in the six Belle $q^2$ bins. The theory predictions are described from Ref. [71].

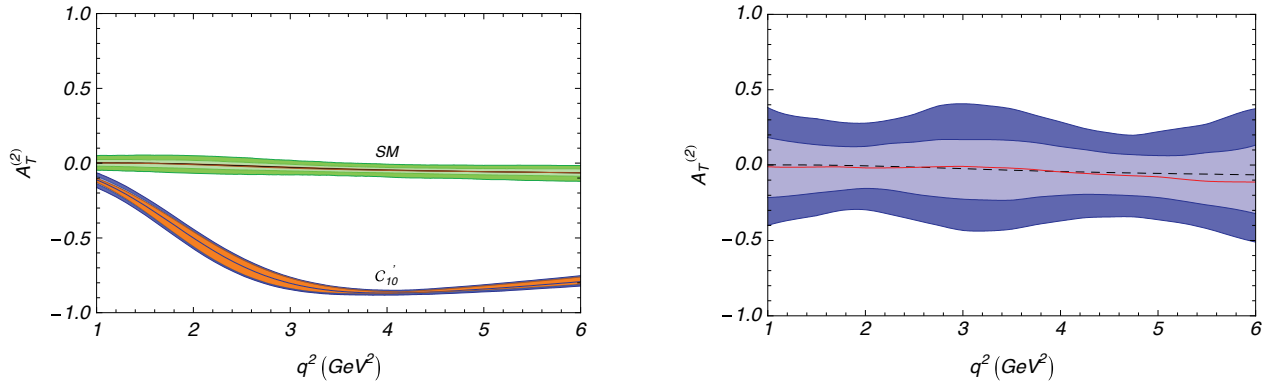


Figure 2.13: (Left) $A_T^{(2)}$ in the SM in green and with NP in blue. The inner line corresponds to the central value of each curve. The dark orange bands surrounding it are the NLO results and the external dark green/blue bands correspond to a 10% correction for each spin amplitude. (Right) expected experimental sensitivity, assuming the SM central values. The inner and outer bands correspond to $1\sigma$ and $2\sigma$ statistical errors with a yield corresponding to a 10 fb$^{-1}$ data set from LHCb.

sample will be necessary in order to probe the full parameter space. These measurements can only be performed at the upgraded LHCb experiment, since no other experiment can reach the necessary level of statistics.

Among related modes, several provide interesting complementary NP searches. The forward-backward asymmetry in $B^+ \to K^+\mu^+\mu^-$ is zero in the SM, but can take different values in models with new scalar or pseudoscalar couplings to the leptons [74]. It is also of interest to study the ratio $R_K = \mathcal{B}(B^+ \to K^+e^+e^-)/\mathcal{B}(B^+ \to K^+\mu^+\mu^-)$, which is equal to unity to good accuracy in the SM, and can be affected by NP [75]. Signals for the $B^+ \to K^+\mu^+\mu^-$ decay have already been seen by LHCb, as shown in Fig. 2.14. Similarly, the $B^+ \to K_1^+\mu^+\mu^-$ and $B^0 \to K_2^{*0}\mu^+\mu^-$ decays provide means to search for NP effects when the meson in the final state is an axial-vector or a tensor, respectively. Similarly, the baryons involved in $\Lambda_b \to \Lambda^{(*)}\mu^+\mu^-$ provide another handle on potential NP amplitudes. The unique feature of $B_s \to \phi\mu^+\mu^-$ is

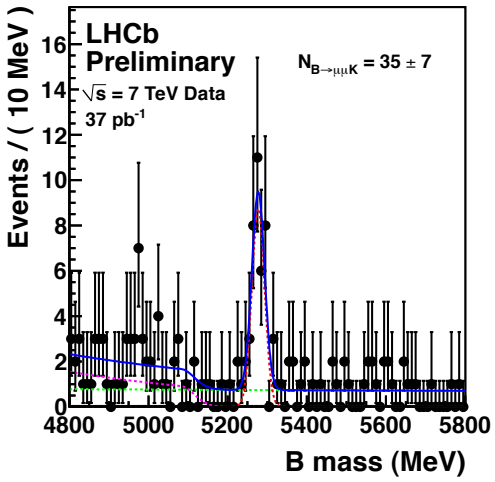


Figure 2.14: Signal for $B^+ \to K^+\mu^+\mu^-$ seen in $\sim 37$ pb$^{-1}$ of LHCb data.

that it allows $CP$ violation in interference between mixing and decay amplitudes to be probed. The upgraded LHCb experiment has unsurpassed potential for all of these analyses.

**Measurement of photon polarisation in exclusive $b \to s\gamma^{(*)}$ decays**
Since $b \to s\gamma$ is a theoretically clean flavour changing neutral current transition, decays mediated by this amplitude are highly sensitive to NP. (We include here the $K^*e^+e^-$ final state.) One particularly interesting feature of this system is that in the SM, the emitted photon is highly polarised. However, this is not the case in extensions of the SM that introduce new right-handed currents. It is therefore of great importance to measure the emitted photon polarisation, which is an experimental challenge.

One particularly promising approach is to study the time-dependent decay distribution of $B_s \to \phi\gamma$ [76]. The key feature of the analysis is that if the emitted photons are polarised, there is no interference between $B_s$ and $\bar{B}_s$ decays (since the final states are, in principle, distinguishable). However, if the photons are not fully polarised, $CP$ violation effects can occur at rates that depend on the level of polarisation as well as on the weak phase. Two particularly attractive features of the analysis of $B_s \to \phi\gamma$, compared to similar measurements in the $B^0$ system, are that (i) the $\phi \to K^+K^-$ decay provides a clean signature, with the tracks originating from the $B_s$ vertex; (ii) the sizable $B_s$ width difference allows the measurement of both $S_{\phi\gamma}$ and $\mathcal{A}^{\Delta\Gamma}_{\phi\gamma}$ (defined in Eq. 2.1) [77]. These are proportional to $\sin 2\psi \sin 2\beta_s$ and $\sin 2\psi \cos 2\beta_s$ respectively, where $\tan\psi$ describes the polarisation ($\tan\psi = 0$ for fully polarised decays). Hence the polarisation can be measured even if the weak phase $2\beta_s$ is small, as in the SM.

LHCb expects a yield of 5.5k $B_s \to \phi\gamma$ events in 1 fb$^{-1}$ of data with a background to signal ratio $< 0.6 - 0.9$ at 90% C.L. [11]. The related decay $B^0 \to K^{*0}\gamma$ has already been seen in LHCb data, as shown in Fig. 2.15. The data from the first phase of LHCb operation will allow the photon polarisation to be measured to about 0.10. This will be a significant improvement on the existing measurements by the B-factories using $B^0 \to K_S\pi^0\gamma$ [45], but will still leave a large region of phase space unexplored. The analysis will benefit maximally from the flexible software trigger of the LHCb upgrade, allowing data samples of over 40,000 $B_s \to \phi\gamma$ decays to

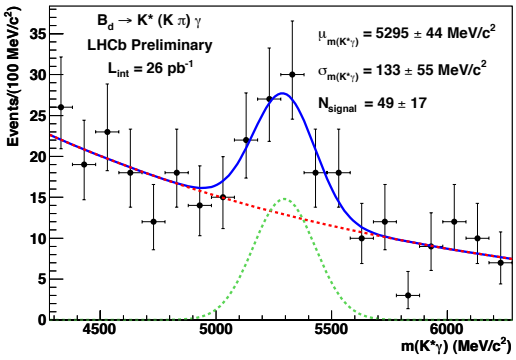


Figure 2.15: Signal for $B^0 \to K^{*0}\gamma$ seen in $\sim 26$ pb$^{-1}$ of LHCb data.

be collected per year. With 50 fb$^{-1}$ of data, the sensitivity to the photon polarisation will be improved to the percent level, and will probe the theoretically most interesting region of phase space.

Other approaches to determine the photon polarisation are also under study. The decay $B^0 \to K^{*0}e^+e^-$ at low values of the dilepton invariant mass-squared (either via virtual photons or by real photons converting in detector material) can be used [78]. Another approach uses analysis of the multibody final state in $B^+ \to K_1^+\gamma \to K^+\pi^+\pi^-\gamma$ [79]. A similar analysis of $B^+ \to \phi K^+\gamma$ decays has also been proposed [80]. All of these analyses are well-suited for the upgraded LHCb experiment.

**Rare hadronic $B$ decays**

Finally, it is worth noting that there are several rare hadronic $B$ decays that are of considerable theoretical interest, for which only the LHCb upgrade will provide sufficient statistics to allow useful measurements. For example, pure annihilation decays such as $B^+ \to D^+K^{*0}$ and $B^+ \to D_s^+\phi$ could be observed at their SM branching fractions with the LHCb upgrade [81]. These observations would provide unique insight into the dynamics of hadronic $B$ decays.

Similarly, the isospin violating decays $B_s \to \phi\rho^0$ and $B_s \to \phi\pi^0$ provide a clean handle on electroweak penguin decays [82]. The branching fractions for these decays are $\mathcal{O}(10^{-7})$ in the SM, but can be significantly modified in various NP scenarios, for example those with extended gauge sectors (i.e. with a $Z'$ boson). These decays can only be studied at LHCb, and require the flexible software trigger of the upgraded experiment.

On the other hand, the decays $B^+ \to K^+K^+\pi^-$ and $B^+ \to K^-\pi^+\pi^+$ are negligibly small in the SM, but can be enhanced by NP to observable levels. These rare decays are complementary to $B^0$ and $B_s$ oscillations in providing sensitivity to NP at very high energies [83].

### 2.1.5 Charm physics

The study of charm is an essential component in the flavour physics programme. The extremely small level of $CP$ violation expected in charm mixing and in decays offers the opportunity for very sensitive null tests of the CKM picture to be performed. Many New Physics models predict significant enhancement in these quantities, as well as distinctive correlations between observables in the charm sector and those accessible in the $B$ system [84]. Charm therefore is

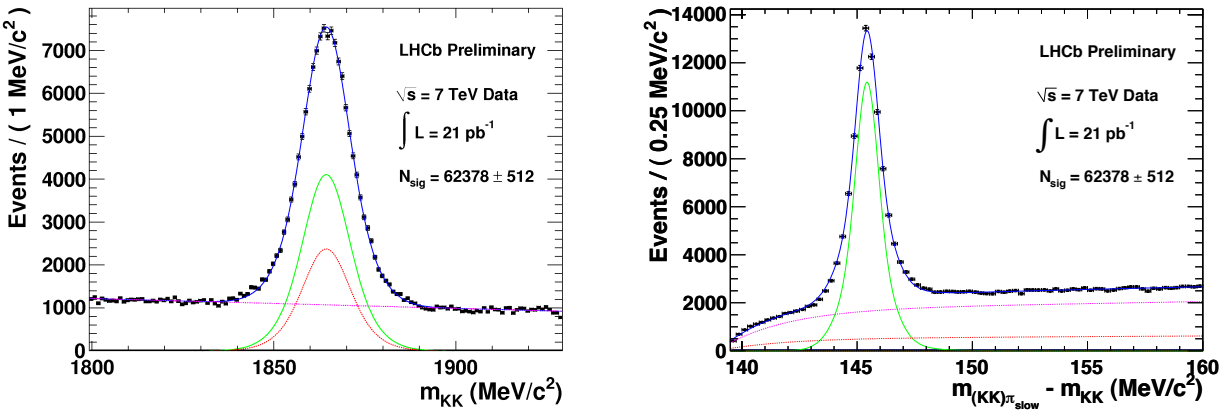


Figure 2.16: The $D^0$ mass and $D^{*+} - D^0$ mass distributions for $D^{*+} \to D^0\pi^+$, $D^0 \to K^+K^-$ events (plus charge conjugate) for 21 pb$^{-1}$ of 2010 LHCb data.

a laboratory in which New Physics can both be discovered, and its nature characterised.

Outstanding charm physics will be performed with the present LHCb detector. Already with the 37 pb$^{-1}$ of data collected during the 2010 run the experiment has accumulated samples of $D^0 \to h^+h^-$ decays of similar size to those of the $B$-factories. These samples are of high purity, as can be seen in Fig. 2.16 for the example mode $D^{*+} \to D^0\pi^+$, $D^0 \to K^+K^-$. The yields in higher multiplicity modes are however significantly lower, due to the constraints of enforcing a $p_{\rm T}$ requirement at the earliest trigger level, with a threshold that is tuned to the needs of $B$ physics. The full software-based trigger strategy of the upgraded detector, however, will allow decays of all topologies to be selected with high efficiency.

The upgraded detector will accumulate yields of $D$ decays that are two-to-three orders of magnitude larger than those collected at BABAR and Belle. These enormous samples will allow for a dramatic improvement in sensitivity to the mixing-related $CP$-violating parameters $\phi_D$ and $(|q/p|_D - 1)$ which are currently measured to be $-0.18 \pm 0.16$ and $-0.10 \pm 0.18$ respectively [45]. Similar improvements will also come in the search for direct $CP$-violating effects, which are final state specific, and are most promisingly searched for in singly-Cabibbo suppressed decays [85]. In such modes Standard Model $CP$-violation may occur at the $10^{-3}$ level, whereas the statistical precision of the LHCb measurements will be $10^{-4}$. Therefore it will be essential to study these effects across a wide range of decays in order to categorise the underlying physics.

There are good reasons to believe that the enormous statistical power of the upgraded experiment can be complemented by the necessary control of systematic uncertainties. In time-dependent analyses the excellent resolution of the detector will contribute negligible uncertainty, in contrast to the situation at $e^+e^-$ machines. The backgrounds lying under the signal peaks are already known to be low, and can be understood from side-band studies. Since biases such as detection asymmetries can be measured from data, it can be assumed that the understanding of these effects will improve in step with the increased statistical precision. Finally, many analyses can be pursued which are intrinsically robust against both experimental and theoretical uncertainty. A few examples are listed below.

- The observable $A_\Gamma$, which is the lifetime asymmetry between $D^0 \to K^+K^-$ and $\overline{D}^0 \to$

$K^+K^-$ decays, probes $CP$-violation in mixing-related phenomena, and is not biased at first-order by any acceptance effects.

- The *difference* in the raw time-integrated $CP$-asymmetry between $D^0 \to K^+K^-$ and $D^0 \to \pi^+\pi^-$ provides a probe of direct $CP$-violation that has *no* systematic uncertainty arising from production or detection efficiencies.

- Dalitz plot analyses provide a sensitive and systematically robust way both to search for and measure $CP$-violating effects. Direct $CP$ violation can be probed for in singly-Cabibbo suppressed decays, such as $D^+ \to K^+K^-\pi^+$ in a model independent manner [86], and exploiting Cabibbo-favoured modes such as $D_s \to K^+K^-\pi^+$ and $D^+ \to K^-\pi^+\pi^-$ for systematic control. In four-body modes such as $D^0 \to K^+K^-\pi^+\pi^-$ measurements exploiting $T$-odd correlations [87] are also model independent and experimentally robust.

- Similarly the $CP$-violating parameters $\phi_D$ and $(|q/p|_D - 1)$ can be measured from a time-dependent analysis in $D^0 \to K^0_S h^+h^-$ decays in a model independent binned fit [88], making use of strong-phase measurements that already exist from CLEO-c [89] and will be further improved at BES-III.

The upgraded detector will also allow for improved sensitivity to important rare charm decays. The present experimental upper limit on the branching ratio for $D^0 \to \mu^+\mu^-$ is $1.4 \times 10^{-7}$ at the 90% C.L. [90], still six orders of magnitude above the Standard Model prediction [91]. Significant enhancements to this decay may come about through R-parity violating supersymmetry [91] or the contribution of leptoquarks [92]. Similar possibilities exist with the lepton-flavour violating decay $D^0 \to e^\pm\mu^\mp$. These super-rare or forbidden modes will be searched for with a sensitivity far in excess of that achievable at present facilities. Other less suppressed decays such as $D^0 \to \rho\mu^+\mu^-$ and $D^+ \to \pi^+\mu^+\mu^-$ may possibly be first observed with the existing detector. However the high statistics that the upgraded experiment will accumulate will allow kinematic distributions to be mapped out in detail, such as the lepton forward-backward asymmetry and the invariant mass spectrum of the dimuon pair, which are powerful discriminants between the Standard Model and New Physics [91].

## 2.2 Lepton Flavour Physics

One of the most promising frontiers to explore in the hunt for NP is that of flavour violating phenomena in the lepton sector. Neutrino oscillations are now an established experimental fact, but the very low mass scale of neutrinos remains to be understood. NP models predict the existence of flavour-violating charged lepton decays, but no such decays have so yet been observed. The upgraded LHCb detector can make significant contributions to these studies, through the search for heavy Majorana neutrinos and lepton flavour-violating $\tau^-$ decays.

### 2.2.1 Searches for $\sim 1$ GeV Majorana neutrinos

The existence of heavy Majorana neutrinos is a natural occurrence in a wide range of models, from left-right symmetric gauge theories [93], to those with extra dimensions [94]. In most models it is quite possible for these particles to exist in the $\sim 1$ GeV/$c^2$ mass range. One

Figure 2.17: Constraints on the sterile-to-active neutrino mixing angle squared, $U^2$, and on the sterile neutrino lifetime, $\tau_N$. These come from the baryon asymmetry of the Universe (solid lines); from the see-saw formula (dotted line); and from requiring Big Bang nucleosynthesis (dotted line). These constraints are shown for the case of an inverted hierarchy in the active neutrino sector. The regions excluded by direct experimental searches are indicated by the blue dashed lines [101,102]. The pink and red curves indicate the expected sensitivity of the proposed LBNE detector at FNAL in two possible configurations.

interesting example is the "Neutrino Minimal SM" ($\nu$MSM) [95], in which such a scenario is indeed preferred. Majorana neutrinos of mass $\sim 1$ GeV/$c^2$ can be searched for in decays of $D$ and $B$ mesons, and constitute an exciting physics goal for an upgraded LHCb experiment.

In the $\nu$MSM three Majorana singlet fermions are added to the SM particles. The lightest of the three new leptons is expected to have a mass of 1–50 keV/$c^2$ and would form a viable dark matter candidate. The two other neutral fermions, which are essentially heavier, sterile neutrinos, can give masses to the SM neutrinos via the see-saw mechanism at the electroweak scale. They would also play a key role in generating the baryon asymmetry of the universe (for a review see [96]). Thus the $\nu$MSM is able to explain three known deficiencies of the SM (dark matter, the baryon asymmetry of the universe and the problem of neutrino mass), and has the further appealing feature that every left-handed fermion then has a right-handed counterpart. The masses of these heavy sterile neutrinos and their coupling to ordinary leptons are constrained by direct searches at particle physics experiments and, importantly, by cosmological considerations, as shown in Fig. 2.17. The requirement that baryogenesis occurs necessitates that the masses of the heavier two neutrinos be almost degenerate and $\mathcal{O}(1)\,\text{GeV}/c^2$ [97].

A powerful approach to searching for $\sim 1$ GeV/$c^2$ Majorana neutrinos is in the decay of heavy flavours [98–100]. Two main strategies exist that are accessible to LHCb:

1. **Direct search**: looking for long lived neutrinos produced in the decay of $D$ and $B$ mesons;

2. **Indirect search**: looking for production of same-sign charged leptons in $D$, $B$ and $\tau$ decays.

Both of these methods are well suited to the upgraded experiment, the former on account of the benefits that a fully software trigger will bring to the search, the latter because of the very large data samples that will be accumulated, allowing for very low branching ratios to be accessed.

**Direct search** Sterile neutrinos could be produced in the weak decays of charm and beauty hadrons, in which mixing occurs between the SM neutrinos and the new particles. Relevant examples of two- and three-body decays are shown in Fig. 2.18. The presence of the massive sterile neutrinos in the decay eliminates the chirality suppression that would otherwise be present. Interesting branching ratios therefore start at the level of $10^{-7}$ (see [100, 102] for details). Since such sterile neutrinos would be very weakly interacting, they would cover a relatively large distance before decaying, but as long as $\sim 10^{-4}$ or more of decays occur within 0.5 m of the production point, this signature would be observable with the upgraded experiment, where the software trigger would provide excellent efficiency for the long lifetime and distinctive topology. Charm decays would provide higher sensitivity for lower mass neutrinos.

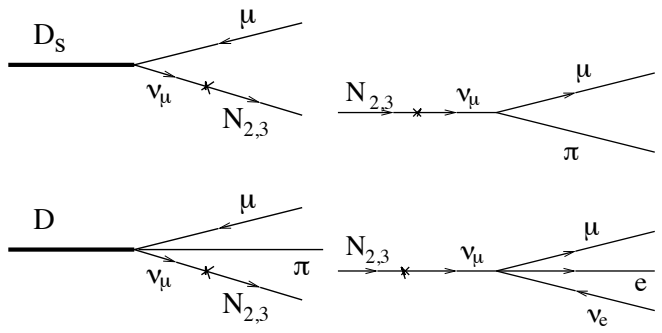


Figure 2.18: Left: Feynman diagrams of charm meson decays producing heavy sterile neutrinos. Right: Feynman diagrams of sterile neutrino decays.

**Indirect search** Heavy sterile neutrinos could also be probed by searching for resonant contributions to lepton number violating processes such as $D_s^{\pm} \to \pi^{\mp}\ell^{\pm}\ell^{\pm}$ or $B^{\pm} \to \pi^{\mp}\ell^{\pm}\ell^{\pm}$ [98,99], as indicated in Fig. 2.19. Here the heavy quark annihilates with the spectator antiquark to

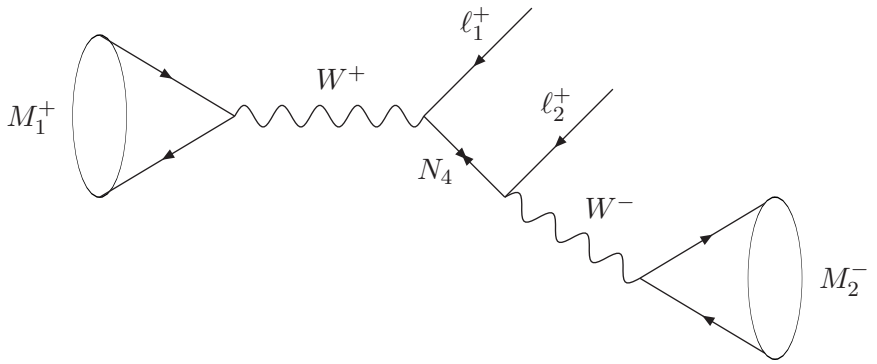


Figure 2.19: The Feynman diagram for meson decay via a lepton number violating process involving Majorana neutrinos. From Ref. [98].

produce a virtual $W$ that can form a lepton-neutrino pair. Assuming so far only SM neutrinos, this process has been used to measure decay constants in such processes as $D_s^+ \to \mu^+\nu$ or constrain CKM elements and charged Higgs contributions in the decay $B^- \to \tau^-\nu$. If, however, the neutrino is Majorana, it can mix into a heavier neutrino that can decay into the same sign $W$ as it was produced in association with, and the $W$ can transform into a like-sign lepton and a hadron, as indicated in the figure. (In this figure and Fig. 2.20 $N_4$ indicates a fourth Majorana neutrino with mass $m_4$ at the GeV scale.) Looking for such a signature is analogous to laboratory based experiments which search for neutrino-less double $\beta$-decay.

The branching ratio of such decays is suppressed by the mixing between the light flavour and heavy neutrinos, $V_{\ell N}$. In the sterile neutrino mass range of $\mathcal{O}(1)$ GeV/$c^2$ accessible with $B$ decays, strong constraints on $V_{eN}$ are imposed by the non-observation of neutrino-less double beta decay ($|V_{eN}|^2 < 10^{-7}$). Searches for the decay products of heavy sterile neutrinos at LEP constrain the equivalent mixing angle for muons, $V_{\mu N}$, to be $|V_{\mu N}|^2 < 10^{-4}$. This could give branching ratios for decays such as $B^{\pm} \to \pi^{\mp}\mu^{\pm}\mu^{\pm}$ at the level of $10^{-8} - 10^{-9}$ which would be accessible at an upgraded LHCb. Other beauty and charm hadron decays can be included in the search. A particularly attractive choice is the mode $B^{\pm} \to D_s^{\mp}\mu^{\pm}\mu^{\pm}$ where the backgrounds

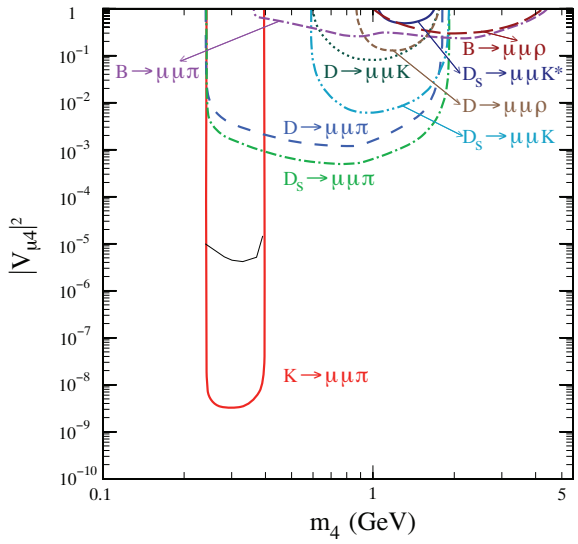


Figure 2.20: Existing bounds on $|V_{\mu 4}|^2$ versus $m_4$ from meson data, from Ref. [98].

are expected to be very low, allowing the statistical power of the upgraded experiment to be fully exploited. Existing bounds in coupling-mass space from heavy flavour decays are shown in Fig. 2.20.

### 2.2.2 Lepton flavour-violating $\tau^-$ decays

No lepton flavour-violating tau or muon decay has yet been observed. Such decays are forbidden in the classical SM, are vanishingly small in the SM extended to include neutrino mixing, but can be enhanced up to observable values in many NP models. The LHC is a prolific source of $\tau$ leptons, with an expected production cross-section of $\sim 0.1$ mb at $\sqrt{s} = 14$ TeV. The majority of produced $\tau$ leptons come from the decay of $D_s$ mesons and $B$ hadrons. The LHCb upgrade will use this sample to search for lepton flavour violating decays to charged track final states.

The current 90% C.L. upper limits from the $B$-factories on branching ratios for the channels $\tau^\mp \to \mu^\mp\gamma$ and $\tau^\mp \to \mu^\mp\mu^+\mu^-$ are at $4.4 \times 10^{-8}$ and $2.1 \times 10^{-8}$ [103]. In supersymmetric extensions of the SM, e.g. in the so-called constrained MSSM, lepton flavour violation in $\tau$ decays is predicted at a level of $10^{-9}$ for $\tau^\mp \to \mu^\mp\gamma$ and at $10^{-10}$ to $10^{-12}$ for $\tau^\mp \to \mu^\mp\mu^+\mu^-$ and $\tau^\mp \to \mu^\mp e^+e^-$ [104]. In other models, such as the so-called Non Universal Higgs Masses (NUHM) SUSY scenario, or the MSSM with R-parity violation and the Little Higgs Models with T parity (LHT) or $Z'$ models with non-vanishing LFV couplings, the rate of $\tau^\mp \to \mu^\mp\mu^+\mu^-$ can be enhanced to the extent that it matches or even exceeds $\tau^\mp \to \mu^\mp\gamma$ [105].

Sensitivity studies for $\tau^\mp \to \mu^\mp\mu^+\mu^-$ are ongoing. With the existing analysis strategy LHCb will be able to match the B-factory sensitivity with a few fb$^{-1}$. The very large integrated luminosity that will be collected by the upgraded experiment will provide a sensitivity corresponding to an upper limit of the order of $10^{-9}$. Searches will also be conducted in modes such as $\tau^\mp \to \mu^\mp\phi$ where the existing limits are much weaker, and very low contamination is expected in the LHCb sample.

Finally, searches will be performed for decays such as $\tau^\mp \to \mu^\mp h_1^\pm h_2^\pm$ ($h_i = \pi, K$). The

physics interest of these topologies is identical to those meson decays discussed in Sec. 2.2.1. The best limit obtained from the B-factories is $3.7 \times 10^{-8}$ for the mode $\tau^{\mp} \to \mu^{\pm}\pi^{\mp}\pi^{\mp}$ [106]. The upgraded LHCb experiments will be able to attain an order of magnitude higher sensitivity.

## 2.3 Physics Beyond Flavour

An upgraded LHCb has the potential to make important contributions to non-flavour physics. The forward-acceptance, flexible software trigger, powerful vertexing and particle identification capabilities provide the experiment with the opportunity to perform very significant measurements in topics far beyond the core programme, and high sensitivity in certain direct particle searches. A few illustrative examples are now given, selected from the diverse areas of electroweak physics, exotic searches, and QCD.

### 2.3.1 Electroweak physics

Two of the most important quantities in electroweak physics are the sine of the effective electroweak mixing angle for leptons, $\sin^2\theta^{\rm lept}_{\rm eff}$, and the mass of the $W$-boson, $m_W$. Until the ILC or CLIC is operational, responsibility for improving our knowledge of these parameters rests with the LHC. Thanks to its unique forward coverage, an upgraded LHCb can make critical contributions to this programme.

The value of $\sin^2\theta^{\rm lept}_{\rm eff}$ can be extracted from $A_{\rm FB}$, the forward-backward asymmetry of leptons produced in $Z$ decays. The raw value of $A_{\rm FB}$ at the LHC is about five times larger than at an $e^+e^-$ collider and so, in principle, it can be measured with a better relative precision, given equal amounts of data. The measurement however requires knowledge of the direction of the matter and antimatter partons that created the $Z$ boson, and any uncertainty in this quantity results in a dilution of the observed value of $A_{\rm FB}$. This dilution is very significant in the central region, as there is an approximately equal probability for each proton to contain the quark or anti-quark that is involved in the creation of the $Z$, leading to an ambiguity in the definition of the axis required in the measurement. However, the more forward the $Z$ boson is produced, the more likely it is that it follows the quark direction; above rapidities $y > 3$, the $Z$ follows the quark direction around 95% of the time. Furthermore, in the forward region, the partonic collisions that produce the $Z$ are nearly always between $u$-valence and $\bar{u}$-sea quark or $d$-valence and $\bar{d}$-sea quark. The $s\bar{s}$ contribution, with a less well known parton density function (PDF), is smaller than in the central region.

Consequently, the forward region is the optimum environment in which to measure $A_{\rm FB}$ at the LHC. Preliminary studies have shown that with a 50 fb$^{-1}$ data sample collected by the LHCb upgrade, $A_{\rm FB}$ could be measured with a statistical precision of around 0.0004. This would give an uncertainty on $\sin^2\theta_{\rm lept}$ of better than 0.0001, which is a significant improvement in precision on the current world average value. It is also worth remarking that the two most precise values entering this world average at present, the forward-backward $b\bar{b}$ asymmetry measured at LEP ($\sin^2\theta^{\rm lept}_{\rm eff} = 0.23221 \pm 0.00029$), and the left-right asymmetries measured at SLD with polarised beams ($\sin^2\theta^{\rm lept}_{\rm eff} = 0.23098 \pm 0.00026$), exhibit a three-sigma discrepancy [107]. LHCb will be able to clarify this unsatisfactory situation.

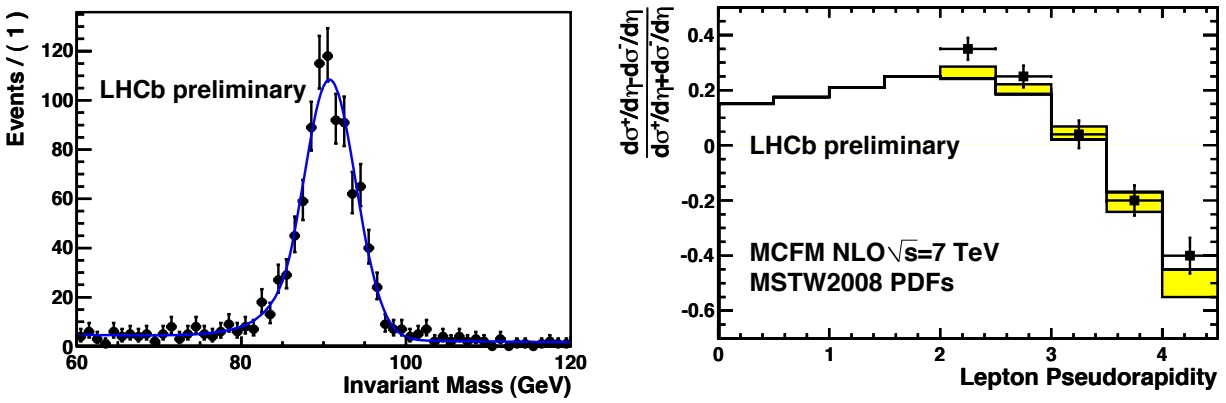


Figure 2.21: LHCb preliminary $Z$ and $W$ results for 16 pb$^{-1}$ at $\sqrt{s} = 7$ TeV. Left: $Z \to \mu^+\mu^-$ peak. Right: $W^+ - W^-$ production asymmetry, where the points with error bars are the data and the boxes are the theoretical predictions with their uncertainties (only indicated within the LHCb acceptance).

More work is needed to identify the important systematic uncertainties on the $A_{\rm FB}$ measurement. One source of error is the uncertainty in the PDFs. With current knowledge this contribution would lead to an uncertainty of almost double the statistical precision estimated above, but this will reduce when the differential cross-section measurements of the $W$ and $Z$ bosons and Drell-Yan lower mass dimuon production measured at the LHC are included in the PDF global fits. LHCb has already embarked on this measurement programme. Figure 2.21 (left) shows the $Z \to \mu^+\mu^-$ peak obtained with 16 pb$^{-1}$ of data. Figure 2.21 (right) shows the measured asymmetry between $W^+$ and $W^-$ production as a function of lepton pseudorapidity. This measurement is already approaching the accuracy of the theoretical uncertainties. The range of the ATLAS and CMS experiments only extends up to lepton pseudorapidities of 2.5.

Decreasing the uncertainty on $m_W$ from its present error of 23 MeV/$c^2$, (which may be reduced further at the Tevatron) is one of the most challenging tasks at the LHC. Although no studies have yet been made of determining $m_W$ with LHCb itself, it is evident that the experiment can give important input to the measurements being made at ATLAS and CMS [108]. A significant and potentially limiting external uncertainty on $m_W$ will again come from the knowledge of the PDFs, and several commentators consider the existing projections to be optimistic [109]. The PDFs are less constrained in the kinematical range accessible to LHCb, and high statistics, precise measurements of $W^+$, $W^-$, $Z$ and low-mass Drell-Yan production in this region, in particular the shapes of the differential cross-sections, can be used to improve the global picture. One specific area of concern arises from the knowledge of the heavy quarks in the proton. Around $20-30\%$ of $W$ production in the central region is expected to involve $s$ and $c$ quarks, making the understanding of this component very important for the $m_W$ measurement. LHCb can make a unique contribution to improving the knowledge of the heavy-quark PDFs by tagging the relatively low-$p_{\rm T}$ final-state quarks produced in processes such as $gs \to Wc$, $gc \to Zc$, $gb \to Zb$, $gc \to \gamma c$ and $gb \to \gamma b$.

### 2.3.2 Exotics

A major goal of experiments at the LHC is to solve the so-called "hierarchy problem": why is the mass of the Higgs boson at the sub-TeV scale, instead of being at the Planck scale, driven there by radiative corrections? Different theoretical paradigms have been proposed, the most discussed being Supersymmetry. There are, however, many other ideas including Extra Dimensions (large, warped, Higgs-less), Technicolour and Little Higgs. These models focus on a strong dynamics type of solution to the problem [110].

A common feature of many such models is the prediction of new states at the TeV scale. In recent years there have been many proposals including $Z'$, 4th quark generation, Leptoquarks, Hidden Valleys, etc. The latter class of models contains low mass states in a new sector with its own quantum number. This new sector is termed the "Hidden Valley", as it lies beyond the energy reach of present experiments. The light states in these hidden sector(s) are connected to the Standard Model sector via massive particles such as the Higgs boson, Supersymmetry sparticles or Kaluza-Klein states of Extra Dimensions. The Hidden Valley class of models is illustrated in Fig. 2.22 where they are labelled "The dark valley Universe" for their possible dark matter content. These models are a very general consequence of string theories [111].

Many proposals exist for the new physics that lies in the hidden valley. A large fraction of these these models predicts the production at the LHC of new particles with long lifetimes, which may decay into $b$-quark jets. These signatures are well suited to LHCb, and in particular the upgraded experiment, which will be able to select events with displaced vertices in the trigger.

Hidden valley particles, or "$v$-flavoured hadrons", can be produced directly via, for example, a Z′. The details of the decay depend on the properties of the hadrons. In one specific model

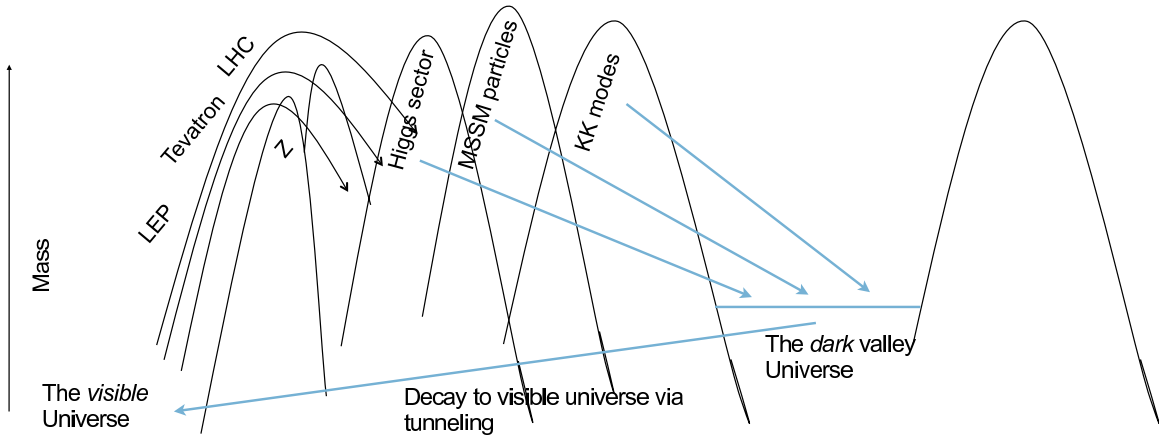


Figure 2.22: An overview of Hidden Valleys. The peaks show possible massive states that could connect the Hidden Sector to Standard Model particles (from Ref. [110]). While the hidden sector is SM neutral, the connector sector is charged under both the SM and the hidden sector.

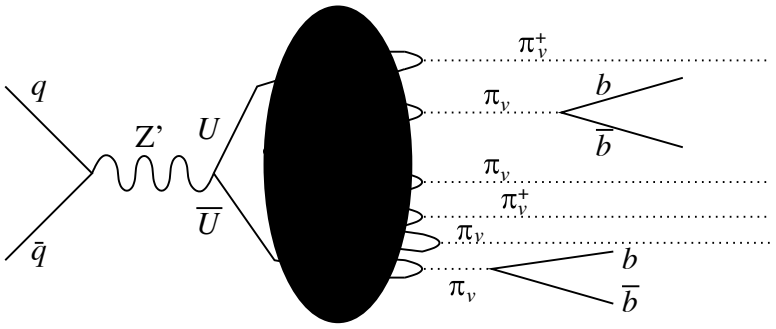


Figure 2.23: Production of electrically neutral $v$-flavored hadrons, $\pi_v$, and their decay. (Taken from [112].)

[112], the $v$-sector contains two new heavy quarks the $U$ and $C$. These can combine, in the case where they are close in mass to form either $v$-isospin 1 hadrons, denoted as either $\pi_v^{\pm}$ for $v = \pm 1$ or $\pi_v^0$ for $v = 0$. All these particles are electrically neutral but the $\pi_v^{\pm}$ hadrons carry '$v$-charge', are stable and constitute dark matter candidates. The 'neutral' member of the isotriplet, the $\pi_v^0$, can decay into ordinary particles. If the mass of the spinless $\pi_v^0$ is below $ZZ$ threshold it will decay dominantly into $b\bar{b}$ pairs due to helicity conservation. Then, as shown in Fig. 2.23, many such $v$ particles can be produced in a single event.

The manifestations of such models are many. Here, by way of example, we discuss a possible scenario in which LHCb would observe the Higgs boson through its coupling to Hidden Valley particles. In Strassler and Zurick [113] it is suggested that the Higgs could decay with a significant branching fraction as follows

$$H^0 \to \pi_v^0 \pi_v^0, \tag{2.8}$$

with each $\pi_v^0 \to b\bar{b}$ as illustrated in Fig. 2.24. Here the $\pi_v^0$ widths are determined by their lifetime which could be very long, resulting in narrow states. The final state would consist of four $b$-jets. If these decays exist, then the lower limit on the Higgs mass set by LEP may be misleading, as it assumes the prompt decay of the Higgs to $b\bar{b}$ to be dominant.

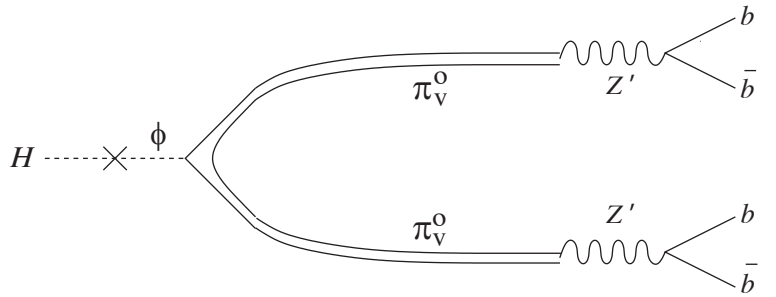


Figure 2.24: Decay of a Higgs via a scalar field $\phi$ into two $\pi_v^0$ particles, with $\pi_v^0$ charge equal to zero, that subsequently decay into $b\bar{b}$ jets. (Taken from [113].)

To investigate the potential of LHCb to search for these exotic Higgs decays a simulation has been performed, assuming an average of 0.4 interactions per crossing, basing the trigger

and subsequent analyses on the following set of cuts: (1) consider events with at least two reconstructed secondary vertices; (2) use only charged tracks from a jet that are consistent with coming from a secondary vertex; (3) require that the two dijet masses should be equal within $3\,\sigma$. The invariant jet masses are computed for events passing this selection.

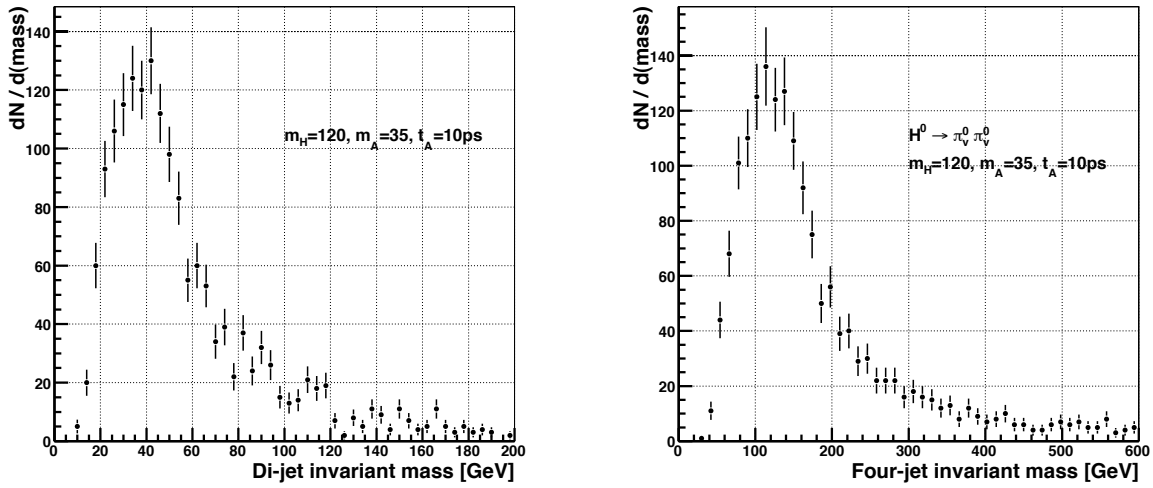


Figure 2.25: Results of signal simulation of the process $H \to \pi_v^0\pi_v^0$, $\pi_v^0 \to b\bar{b}$. Left: Reconstructed dijet invariant mass. Right: the mass of both dijets, that peaks at the putative Higgs mass; here two equal dijet masses are required. The input masses to the simulation are 35 GeV/$c^2$ for the $\pi_v^0$ and 120 GeV/$c^2$ for the Higgs.

In Fig. 2.25 the distributions are shown for both the invariant mass of the dijets (left), and for the four-jet invariant mass (right) for those combinations where the dijet masses are very similar (right). The input parameters for the simulation are $\tau_{\pi_v^0} = 10$ ps, $m_{\pi_v^0} = 35$ GeV/$c^2$ and a Higgs mass of 120 GeV/$c^2$. No generator information has been used in the analysis or reconstruction. For both the dijet and four-jet reconstruction peaks are evident close to the correct mass. It will be possible to improve further by refining the jet definition and calibration, and by imposing constraints, for example that the masses of the two $\pi_v^0$ candidates be equal.

Assuming a Higgs production cross-section at 14 TeV of 50 pb, an integrated luminosity of 50 fb$^{-1}$ and a geometric efficiency of 10%, 250,000 Higgs bosons will be produced in LHCb. If $H^0 \to \pi_v^0\pi_v^0$ is a dominant decay mode, then LHCb will be in an excellent position to observe this signal, taking advantage of the software trigger's ability to select high multiplicity events with good efficiency. Backgrounds to this signal from other processes, such as the production of two pairs of $b\bar{b}$ quarks, have been considered and found to be negligible.

Long-lived particles, which would give rise to secondary vertices that would be a suitable signature for the trigger of the upgraded experiment, are found in many Supersymmetric theories. Examples include the bilinear R-parity violating SUSY models of de Campos *et al.* [114] that predict long-lived SUSY particles such as neutralinos decaying into $W$ + lepton, or $Z$ + $\nu$, or $b\bar{b}$+ $\nu$, and the proposal of Carpenter *et al.* [115], in which the Higgs dominantly decays to a pair of long-lived neutralinos, each of which subsequently decays to three quark jets.

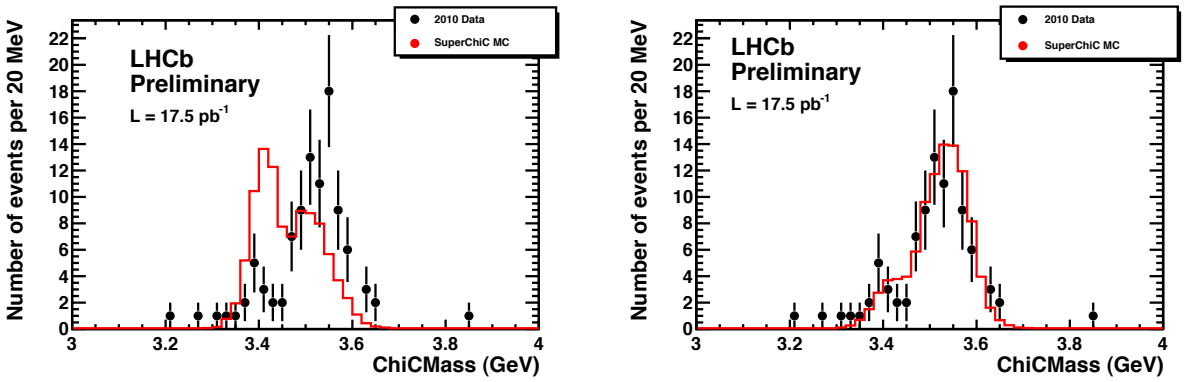


Figure 2.26: Preliminary LHCb results on central exclusive $\chi_c$ production. Also shown is the expectation of the SuperCHIC Monte Carlo [119], which has been normalised to the number events observed in the data. The relative proportions of $\chi_{c0}$, $\chi_{c1}$ and $\chi_{c2}$ in the Monte Carlo are 52%, 36% and 12% respectively in the left plot, and 12%, 36% and 52% respectively in the right plot. (The data points are the same.)

### 2.3.3 Central exclusive production

Central exclusive production (CEP) processes provide a promising and novel way to study QCD and the nature of new particles, from low mass glueball candidates up to the Higgs boson itself. The CEP of an object $X$ in a $pp(\bar{p})$ collider may be written as follows

$$pp(\bar{p}) \to p + X + p(\bar{p}),$$

where the + signs denote the presence of a large rapidity gap. At high energies the $t$-channel exchanges giving rise to these processes can only be zero-charge colour singlets. Known exchanges include the photon and the Pomeron. Another possibility, allowed in QCD, but not yet observed, is the Odderon, a negative $C$-parity partner to the Pomeron with at least three gluons. The most attractive aspect of CEP reactions is that they offer a very clean environment in which to measure the nature and quantum numbers of the centrally produced state $X$.

Central exclusive $\gamma\gamma$ [116], dijet [117] and $\chi_c$ [118] production has been observed at the Tevatron. Already in the 2010 run LHCb has collected candidate dimuon events compatible with CEP. In Fig. 2.26 the invariant mass of CEP $\chi_c$ candidates is shown. These are events in which only a $J/\psi \to \mu^+\mu^-$ decay and $\gamma$ candidate are reconstructed, with no other activity (inconsistent with noise) seen elsewhere in the detector. An important observable in CEP is the relative production rates of $\chi_{c0}$, $\chi_{c1}$ and $\chi_{c2}$. As is evident from Fig. 2.26, the invariant mass resolution of LHCb is sufficient for this measurement to be made.

These early results make clear the promise of CEP measurements at LHCb. Additional instrumentation can be considered which will help in these studies, should results with the current detector prove interesting. For example, the inclusion of Forward Shower Counters (FSCs) on both sides of the interaction point [120], would be able to detect showers from very forward particles interacting in the beam pipe and surrounding material. The absence of a shower would indicate a rapidity gap and be helpful in increasing the purity of a CEP sample. The deployment of semiconductor detectors very close to the beam within Roman pots, several 100 m away from the interaction point, as proposed for ATLAS and CMS [121] could also be beneficial for LHCb. Several important physics goals may already by identified for the LHCb CEP programme:

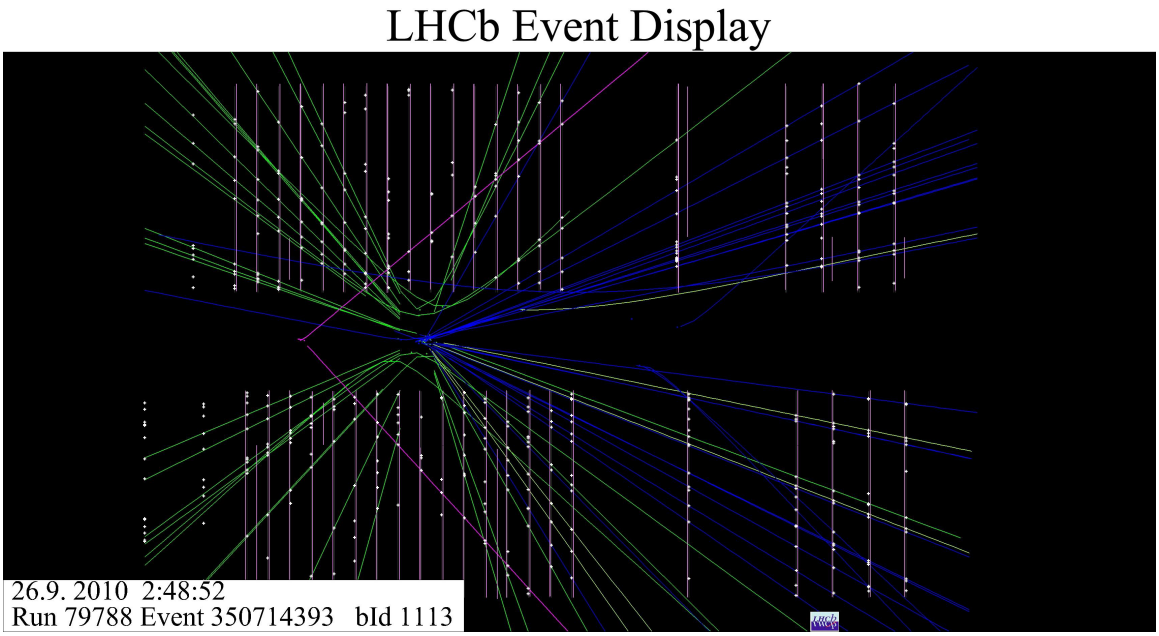


Figure 2.27: Event display in the VELO region of candidate CEP $J/\psi \to \mu^+\mu^-$ event with pile-up. The horizontal scale is 1 m, and the vertical scale is around 8.5 times smaller. The sensors are indicated either side of the beam region, together with the detected hits. Reconstructed tracks are superimposed. A primary vertex arising from one interaction can be seen, slightly left of centre, from which most tracks originate. Left of this (upstream), and clearly isolated, is the vertex of two tracks which form a $J/\psi \to \mu^+\mu^-$ candidate.

- To accumulate and characterise large samples of exclusive $c\bar{c}$ and $b\bar{b}$ events. A full measurement programme of these "standard candles" will be essential to understand better the QCD mechanism of CEP [122], and may provide vital input if CEP is used for studies of Higgs and other new particles [123].

- Searches for structure in the mass spectra of decay states such as $K^+K^-$, $2\pi^+2\pi^-$, $K^+K^-\pi^+\pi^-$ and $p\bar{p}$. A particular interest of this study would be the search for glueballs, which are a key prediction of QCD.

- Observation and study of exotic particles in CEP processes would be illuminating as to their nature. For example, a detailed study of the CEP process $pp \to p + X(3872) + p$ would provide a valuable new tool to test the quantum numbers of this state. This and other states could also be searched for in, for example, decays containing $D\bar{D}$, which if observed would shed light onto the nature of the parent particle [122, 124].

There are several reasons which make LHCb a suitable detector for performing such studies, particularly with the upgraded experiment:

- Even when running at a luminosity of $10^{33}$ cm$^{-2}$s$^{-1}$ LHCb will have much less pile-up than ATLAS or CMS, which will be operating in a much more severe regime. This will be advantageous in triggering and reconstructing low mass CEP states. Not only will there still be a significant fraction of CEP interactions produced in isolation, but it will also prove possible to select CEP interactions in the pile-up environment. This has

already been demonstrated with the 2010 data, as shown in Fig. 2.27, where a $J/\psi$ vertex can be seen completely separated from, and upstream of, the primary vertex of another interaction. The software trigger of the upgrade will be used to select such events, not only containing $J/\psi \to \mu^+\mu^-$ but also two, three and four charged-track CEP decays.

- The higher integrated luminosity that will be collected by the upgraded detector will allow studies to be performed on states that are inaccessible with only a few fb$^{-1}$. This is true, for example, of central exclusive $\chi_b$ production, which is expected to be a factor of $\sim 1000$ down with respect to that of $\chi_c$ mesons [122].

- The particle identification capabilities of the LHCb RICH system allow centrally produced states to be cleanly separated into decays involving pions, kaons and protons.

- The low $p_{\rm T}$ acceptance of LHCb, and high bandwidth trigger, will allow samples of relatively low mass states to be collected and analysed.

# Chapter 3

# Detector

## 3.1 Trigger

The current LHCb trigger architecture [13, 125] has two levels: Level-0 (L0) is a trigger implemented in hardware while the High Level Trigger (HLT) consists of a software application which runs on every CPU of the event-filter farm (EFF). The purpose of L0 is to reduce the rate of crossings with interactions to below a rate at which the HLT can process the events. For the current detector this maximum rate is determined by the front-end (FE) electronics, and is 1.1 MHz. The FE-electronics will be upgraded to allow reading events at the LHC clock rate. In principle the upgrade should allow to perform data acquisition and event building on the EFF at the full rate of 40 MHz. However the upgrade is designed to be able to cope with a staged DAQ system which cannot yet handle the full rate, occupancy fluctuations which prevent the full readout, and insufficient CPU power in the EFF. Hence the upgrade will also contain a Low Level Trigger (LLT), which like L0 should not just pre-scale to a rate acceptable by the DAQ and EFF, but enrich the selected sample with interesting events. The LLT corresponds closely to the current L0, but with a tunable output rate higher than the current 1.1 MHz limit.

During the 2010 and 2011 running the trigger performed as expected [126], but needed to adapt to running conditions which were at times very similar per crossing to those expected for the upgraded LHCb detector. As a result the HLT [127, 128] has evolved significantly from the implementation described in [125], profiting from the excellent detector performance both in efficiency and alignment. The HLT is subdivided in two stages HLT1 and HLT2. HLT1 reconstructs particles in the VELO and determines the position of the primary vertices (PV) in the event. To limit the CPU consumption, a selection of VELO tracks is made based on their smallest impact parameter (IP) to any PV, and their quality. For these selected VELO tracks their track-segment in the T-stations are sought to determine their momentum ($p$), so-called forward tracking. HLT1 selects events with at least one track which satisfies minimum requirements in IP, $p$, $p_{\mathrm{T}}$ and track quality. It reduces the rate to a sufficiently low level to allow forward tracking of all VELO tracks. HLT2 searches for secondary vertices, and applies decay length and mass cuts to reduce the rate to the level at which the events can be written to storage.

The trigger for the upgrade is the basically same as the trigger which LHCb has currently deployed, with the exception of allowing a much larger LLT rate, and correspondingly a much larger rate to storage. Figure 3.1 gives an overview of the trigger levels of the upgrade, the

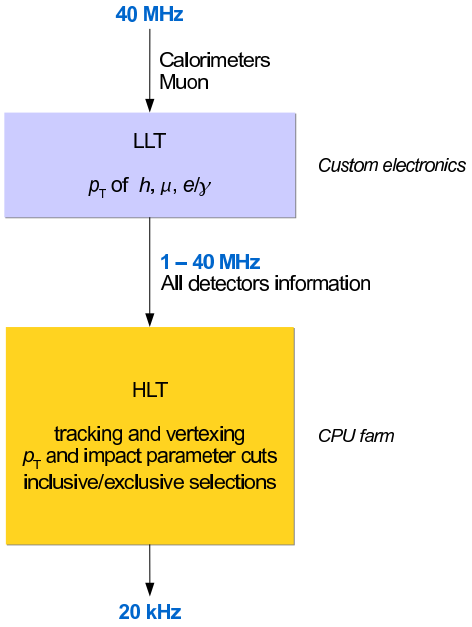


Figure 3.1: Overview of the upgraded LHCb trigger.

components used to select events and the trigger rates. The LLT output rate is expected to typically be between 5–10 MHz, while the rate to storage will be $\sim$ 20 kHz. The expected performance of the overall trigger system at a luminosity of $10^{33}$ cm$^{-2}$s$^{-1}$ is based on trigger code which is actually running in LHCb today.

## 3.2 Electronics

A new electronics architecture is required to satisfy the requirements of reading data from every bunch-crossing in the upgraded LHCb. The existing architecture, as described in [129], includes a Level-0 pipeline buffer and derandomiser. These limit the readout speed and hence the trigger rate to 1 MHz, so any increase beyond 1 MHz requires their removal and a re-design of the electronics. Many of the challenges of the 40 MHz readout scheme can be met by the use of modern technologies adapted for high energy physics. For example, high-speed optical links will be installed to accommodate the increase in data volume from the detector. Data compression

schemes will be implemented on the detectors to minimise the number of these links. Though the aim is to eliminate the hardware-based part of the trigger, a throttling mechanism will be designed to control the data flow into the data acquisition. This throttle can also be enhanced with physics information in a manner similar to the existing LHCb L0 trigger, and is known as the Low Level Trigger (LLT), as discussed in the previous section.

Although the upgrade will require major changes to the electronics of the detector, a number of measures will be taken to minimise cost, development time and installation effort, namely:

1. Re-use parts of the existing front-end electronics that can satisfy the upgrade requirements;

2. Develop common devices and modules to be used by all sub-detectors;

3. Re-use as much of the existing infrastructure as possible.

This section describes the generic electronics architecture and the parts common to all sub-detectors. The general architecture is shown in Fig. 3.2. The front-end (FE) amplifies and shapes the signals generated within the detectors. These signals are digitised, compressed, formatted and then transmitted down a high-speed optical link. The back-end electronics (BE) sit in the counting room and receive the data from the optical links. After buffering and filtering by the LLT, data are formatted for transmission to the data-acquisition system. Data from the Calorimeter and Muon sub-detectors are extracted via an independent transmission system to the trigger processors where the LLT is generated. Transmission of trigger information is through a Timing and Fast Control (TFC) system and takes the form of bunch-crossing identification numbers for which the LLT gave a positive decision. Configuration and monitoring of the BE and FE electronics are through an interface to the Experiment Control System (ECS).

Compression of the data is advantageous for cost reasons, although in some regions of certain detectors the channel occupancy is such that zero-suppression is not economical and will not be used. Following any compression step, a buffer will absorb statistical fluctuations in the data size and allow an optimal use of the data band-width provided by the link. However, this implies that data from different FE modules will arrive asynchronously at the BE modules. Additional information is therefore attached as a header to the data packets to allow selection by the LLT and reconstruction of the complete events. This is based on a bunch-counter within the FE module running synchronously with the LHC clock. If the FE buffer is full, then data will be truncated until the buffer recovers. However, to maintain synchronicity, empty data packets containing only header words will still be transmitted. To minimise the risk of de-synchronisation, resets of the bunch counters will be issued once every orbit of the LHC machine.

The implementation of zero-suppression or data compression in the FE electronics implies that detector parameters such as the channel occupancy must be well understood before the hardware is designed and constructed. The efficiency of the algorithms and the amount of buffering are currently being tested using data from Monte Carlo simulations of the detector at the luminosities foreseen for the upgrade.

The hardware and protocol chosen for the links supports bi-directional transmission. However, the data band-width from the detector far outweighs that for TFC and ECS transmission to the detector. For this reason and to allow a cost-effective modular approach, it has been

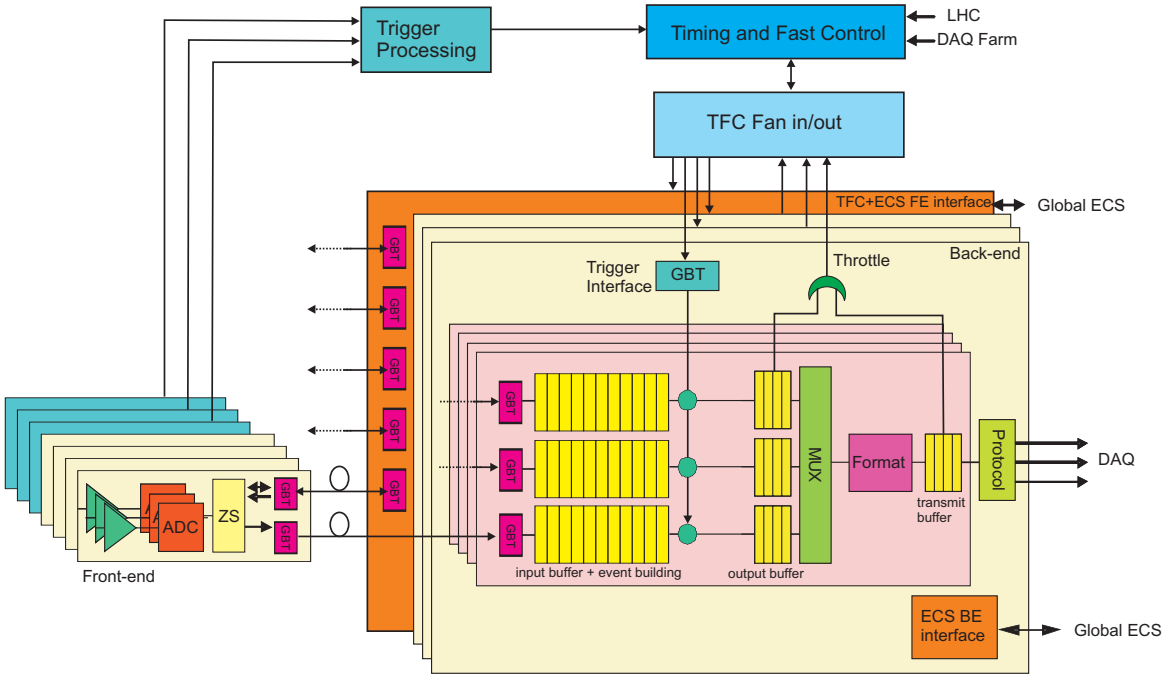


Figure 3.2: The general electronics architecture of the LHCb upgrade.

chosen to use the link in simplex mode for data transmission, and in duplex mode for combined TFC and ECS communication.

## 3.3 Vertex Locator (VELO)

The physics programme of the LHCb upgrade requires an extremely performant vertex detector with fast pattern recognition capabilities, excellent vertex resolution and two track separation, and sufficient radiation hardness to guarantee excellent performance throughout the upgrade data-taking period. In particular, the trigger performance, which relies heavily on the vertex detector data, must be fast and flexible enough to adapt to the evolving physics needs of the experiment. The move to a 40 MHz readout necessitates the construction of a new Vertex Locator (VELO) with appropriate electronics and sufficient radiation hardness. Pixels are an attractive choice for the upgraded VELO due to the high granularity and the relative ease of pattern recognition. In order to provide 40 MHz readout, the Timepix chip, from the Medipix family of chips [130] has been identified as an excellent candidate from which the final pixel FE electronics, dubbed "VELOPIX" could be developed. The principal challenges of the pixel module design are to keep the module sufficiently light and to control the power consumption and cooling to the required levels. The alternative of an upgraded VELO strip detector would be similar to the current VELO design, but require improved cooling and a new ASIC, with possible synergies with the Silicon Tracker upgrade silicon option. For more details about the VELO upgrade see [131].

## 3.4 Charged Particle Tracking

The downstream tracking region of LHCb comprises one tracking station (TT) located upstream, and three tracking stations ("T-stations", T1–T3) at the downstream side of the magnet. The purpose of these tracking stations is twofold:

1. provide a high precision momentum measurement for charged particles resulting in precise mass resolutions of unstable particles;

2. measure the track directions of the charged particles as input to photon-ring searches in the RICH detectors for particle identification.

In the reconstruction sequence of LHCb we distinguish different track-types depending on the sub-detectors they traverse: "long tracks" traverse the full spectrometer (VELO and T-region) and have best momentum and vertexing quality, "downstream tracks" traverse only the TT and T-region and contain good momentum information, and finally "T-tracks" only traverse the T-stations and have precise slope information for RICH-2.

For low and medium momentum tracks (up to about 80 GeV/$c$) the momentum resolution is mainly limited by multiple scattering, while for higher momentum tracks the detector resolution becomes the limiting factor. To measure track momenta of all particles a T-station track-segment after the magnet is used in the following ways.

- For high momentum long tracks, the momentum is effectively measured by combining the T-station segment with a track slope measurement before the magnet using VELO and TT.

- For lower momentum long tracks as well as for downstream tracks, the momentum is effectively determined by combining the T-station segment with a short TT track-stub.

- For T-tracks the momentum is measured either by assuming the track originates from the primary vertex (for high momentum tracks) or by measuring the curvature in the stray magnet-field in the T-region (for low momentum tracks).

To achieve these goals the T-detectors were designed to provide high efficiency standalone pattern recognition capabilities together with high resolution in the B-field bending plane. The T-detectors consist of large Outer Tracker straw detectors, covering 98% of the 30m$^2$ detector surface and smaller Inner Tracker Silicon detectors, covering 0.3m$^2$ at the small angle—high track density—region. The T-stations are used in the HLT to find long track continuations of VELO track-seeds and provide precision momentum information in the trigger to inclusively select signal events. Alternatively, offline standalone track finding in the T-stations complements the track finding to achieve maximum efficiency for exclusive final state reconstruction.

The TT station covers the full acceptance of 2 m$^2$ before the magnet and was constructed using the same Si technology as the IT detector. The purpose of the TT-station is four-fold:

1. To reconstruct the trajectories of long-lived tracks that decay outside the fiducial volume of the VELO detector (e.g. $K_S$ decays).

2. To reconstruct low momentum "slow" particles that bend out of the acceptance of the detector before reaching the T-stations.

3. To provide an additional track segment to ease pattern recognition and to improve the connection between the track segments determined by the VELO and the downstream T-stations. In the present high pile-up data taking mode with high track density in the detector, a significant reduction of false tracks ("ghosts") has been achieved, when tracks are required to be validated by TT hits.

4. To allow for selecting high momentum tracks in an early stage of the online track trigger. Since low momentum tracks may scatter and give rise to a large impact parameter, knowledge of the track momentum suppresses the secondary vertex candidates. This feature is not used at present, since in the region between VELO and TT the multiple scattering is higher and the magnetic field is lower than assumed in the original simulations.

The set-up of the tracking detector stations was designed [132, 133] and optimized [134] to provide best performance in a high track-density environment[1] corresponding to instantaneous luminosities in the range of $\mathcal{L} = 2 - 5 \times 10^{32}\text{cm}^{-2}\text{s}^{-1}$. For nominal LHC running $\mathcal{L} = 2 \times 10^{32}\text{cm}^{-2}\text{s}^{-1}$ corresponds to 10 MHz visible interactions with an average number of 0.4 interactions per bunch crossing. At these run conditions the T-stations are expected to observe on average 72 charged particle tracks, of which 26 are long tracks, for a $b\bar{b}$ event [134].

For optimal track reconstruction, each of the stations is equipped with four measurement layers according to the coordinates: X-U-V-X, where X indicates a horizontal measurement and U and V stereo measurements at $\pm 5°$ from X. The presence of two X-layers allows to perform an initial 2-dimensional track search algorithm as an initial step for a full 3-dimensional pattern recognition procedure. Experience with the HERA-B detector, as well as dedicated MC pattern recognition studies demonstrated that optimal ghost rejection performance was obtained for stereo angles in the region of 2.5° to 7.5°. The choice of a stereo angle of 5° provides a $y$-coordinate measurement with sufficient precision on the track slopes for the RICH pattern recognition [134]. For the TT detector a similar geometry was adopted to ease the reconstruction of $K_S$ decaying downstream of the VELO.

Contrary to the IT, the TT and OT detectors have their on-detector electronics mounted just outside the fiducial volume of the experiment. The read-out systems of the tracking detectors allow T and TT station measurement information to be available in the HLT trigger with a 1 MHz readout frequency.

## 3.5 Particle Identification

The particle identification (PID) system is a vital component of the upgraded LHCb detector. Several key physics channels which involve kaons rely on the RICH PID to reject copious backgrounds from multiple-track combinatorics and events with similar decay topologies. Especially important are the rare decays $B_s \to \phi\phi$, $B_s \to \phi\gamma$, $B \to \phi K^0_S$, as well as the gamma-measurement family of channels $B \to DK$. The PID is also crucial for the kaon tagging performance of the experiment, especially for momenta up to $10\,\text{GeV}/c$.

The baseline PID system will consist of the two existing RICH detectors, to be augmented by a novel detector based on time-of-flight to identify low momentum particles. As for the

[1] For all simulation studies at various luminosities nominal LHC operation with 25 ns bunch spacing and $\sigma_{\text{inel}}(\sqrt{s} = 14\text{ TeV}) = 80$ mb is assumed.

current detector, the key momentum range is from $p \sim 2\,\mathrm{GeV}/c$ up to $\sim 100\,\mathrm{GeV}/c$ [13]. The upstream RICH-1 detector currently has aerogel and $C_4F_{10}$ gas radiators, covering momenta from $\sim 2$ to $10\,\mathrm{GeV}/c$ and $\sim 10$ to $60\,\mathrm{GeV}/c$, respectively. The downstream RICH-2 detector has a $CF_4$ gas radiator and covers momenta up to $\sim 100\,\mathrm{GeV}/c$.

The philosophy adopted has been to re-use as much as possible all existing RICH mechanical and optical components. The current RICH system employs custom-built photon detectors, the Pixel HPDs [135], which operate very successfully. However these cannot be re-used in the upgraded RICH detector since the HPD readout electronics are limited to a 1 MHz event readout rate, incompatible with the upgrade rate of 40 MHz. The fact that the HPD readout chip is integrated within the vacuum envelope of the HPD tube therefore precludes simply replacing the chip and retaining the photon detectors. It is therefore proposed to replace the HPDs with multi-anode photomultipliers (MaPMTs) with external 40 MHz readout electronics.

From simulation studies it has been concluded that the low photon yield of the aerogel radiator (a mean of 5.5 photons per saturated track [13]), coupled with the increased background at high luminosity, will be inadequate in the harsh environment of the LHCb upgrade. This would compromise the crucial low-momentum PID, for which the key physics performance indicators are the same-side kaon (SSK) and opposite-side kaon (OSK) tagging powers in $B_s \to \phi\phi$ events. The presence of aerogel does not improve the tagging performance at high luminosity, nor does it have the necessary robustness. The low-momentum PID efficiency, and robustness at this higher luminosity, can be restored with a time-of-flight system discussed below.

In the current detector, the aerogel is located in the middle of the tracking system, and its removal will reduce the material budget by about 5% of a radiation length. In addition, the aerogel gives much larger rings than the gas radiator of RICH-1, so about half of the photodetector area of RICH-1 is currently devoted to the aerogel. The area to be covered by the upgraded photodetectors of RICH-1 will therefore also be significantly reduced.

In the upgraded detector, it is proposed to remove the aerogel from RICH-1, and instead use a system based on time-of-flight to cover the low momentum range below $\sim 10\,\mathrm{GeV}/c$ (i.e. below the kaon threshold in the $C_4F_{10}$ gas radiator). Three sigma $\pi$/K separation and positive proton separation up to $10\,\mathrm{GeV}/c$ requires a time-of-flight resolution of about 15 ps per track, at a distance of $\sim 10$ m from the interaction region. The proposed detector combines time-of-flight and RICH detection techniques, and is named the TORCH [136]. It relies on the detection of Cherenkov photons from a 1 cm-thick plane of quartz to measure the time-of-flight of tracks. The photons propagate by total internal reflection to the edge of the plane, in a manner similar to a DIRC detector [137]. They are then focused onto an array of Micro-Channel Plate photon detectors (MCPs) at the periphery of the TORCH detector. The time-of-propagation of the photons in the quartz plate also depends on the particle type that produced them, as different velocity particles give a different Cherenkov angle and therefore a different path length. This effect is coherent with the time-of-flight difference, and enhances the separation power. The goal of achieving a time resolution of 15 ps per track, together with the expected number of detected photons per track of around 30, dictates a 70 ps resolution in the single-photon time measurement.

Figure 3.3 shows the calculated performance of the different components of the PID system, for isolated tracks, in terms of the significance (in number of Gaussian sigmas) for K-$\pi$ separation as a function of momentum. Excellent particle identification can in principle be achieved over the full momentum range of interest. The actual performance that will be obtained de-

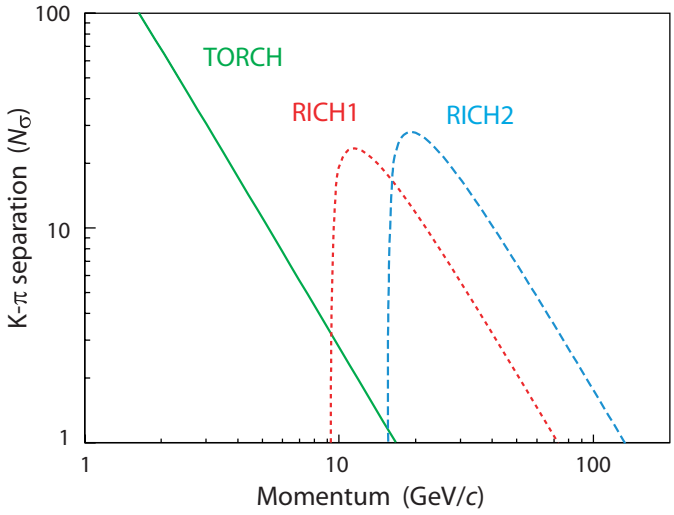


Figure 3.3: Calculated performance (in sigma separation) of the different components of the PID system versus momentum, for isolated tracks. The assumed resolutions per photon and photon yields per track are (70 ps, 1.6 mrad, 0.7 mrad) and (30, 16, 12) for (TORCH, RICH-1, RICH-2) respectively.

pends on the background and pattern recognition, and a preliminary simulation study has been performed.

## 3.6 Calorimetry

The present calorimeter system of LHCb is composed of a Scintillating Pad Detector (SPD), a Preshower (PS), an Electromagnetic Calorimeter (ECAL) and a Hadronic Calorimeter (HCAL). The HCAL is based on the Tilecal technology and contains 1488 cells. It is preceded by the ECAL based on the Shaslik technology and containing 6016 cells. In front of the ECAL, the PS is composed of 6016 tiles matching the geometry of the ECAL. The PS is placed after a lead sheet of 2.5 radiation length and is preceded by another layer of 6016 scintillator tiles, the SPD. The detailed description of the calorimeter system can be found in [138].

The calorimeter system plays a role in photon reconstruction (ECAL), in photon and electron identification (ECAL, PS, SPD), and in the trigger system (HCAL, ECAL, PS, SPD).

For this document we have concentrated the studies on the upgrade of the ECAL and HCAL readout at 40 MHz, since the removal of the SPD and PS is being considered for the upgrade.

- The Low Level Trigger (LLT), foreseen to replace our present L0 trigger, does not require a very strict selection and therefore it can be operated without the PS and SPD.

- It remains to be studied whether the necessary electron and photon identification needed for parts of our upgrade physics program can be achieved without the SPD and PS.

If an upgrade of the SPD and PS is needed, the modifications to the Front-End (FE) cards would be very similar to the modifications of the ECAL/HCAL FE-cards described below.

To minimize the required modifications, it is planned for the upgrade to keep the present ECAL and HCAL calorimeter modules, their photomultipliers (PMT), Cockroft Walton bases

(CW) and coaxial cables. However, to keep the same average anode current of the phototubes at the higher luminosity, their high voltage (HV) is reduced and therefore the gain of the amplifier integrator in the Front-End card will be increased.

The racks and crates situated at the top of the calorimeter can be kept as they are, however of course the FE-cards have to be modified to allow a read out at 40 MHz. To minimize the number of fibres necessary to read the calorimeters, the ADC information is packed using an algorithm similar to the one presently used in the TELL1 calorimeter cards.

The decision to keep the calorimeter modules, their PMTs and CW bases assumes that they can operate with the radiation damage corresponding to the foreseen integrated luminosity.

Because of the higher luminosity, there will be a higher occupancy in the calorimeter cells. This will cause an increase in calorimeter noise due to statistical fluctuation in these underlying events. While the effect is small for the measurement of high $E_{\mathrm{T}}$ photons it is important in the case of low $E_{\mathrm{T}}$ photons.

## 3.7 Muon System

The muon system [13, 139, 140] is the most shielded sub-detector of LHCb and the primary component of particle flux is less dominant than in other subsystems. Nevertheless, ageing of detectors, their rate capabilities, the long term reliability of the present electronics and the performances of muon identification in a high rate environment are concerns for the system when operated with a luminosity of $10^{33}$ cm$^{-2}$s$^{-1}$. Muon station M1 will not be needed in the upgrade, as the improvement in the Low Level Trigger (LLT) muon momentum resolution will be performed by the tracking stations, and the expected high rate will make it less useful.

Most of the hits recorded by the muon chambers in the stations M2–M5 are produced by secondary particles coming from electromagnetic and hadronic showers and by the low energy neutron background. The actual values of these components, simulated in the LHCb Monte Carlo with safety factors, have been studied in the first year of operation of the detector.

The muon system Front-End (FE) electronics is already read out at 40 MHz, as it is currently sending data at this rate to the L0 trigger, while the full TDC information is sent at 1 MHz to the DAQ system. This scheme has to be slightly modified, in order to have a system fully integrated with the general LHCb LLT and with the rest of the upgraded DAQ. As a global strategy, it is planned to have a minimal set of changes for the muon system and its FE-electronics.

A key element for a successful running of the system at high luminosity will be a good understanding of the high rate performance of the MWPCs and of detector ageing effects. detector operation stability, considerations about spare chambers and ongoing R&D of large-area GEM detectors.

## 3.8 Online system and Offline computing

The Online system consists of the Experiment Control System (ECS), the Timing and Fast Control (TFC), the Data Acquisition (DAQ) and the Online IT infrastructure (OIT).

The architecture and the basic principles were described in the LHCb Online TDR [141]. They are: a unified control system for all hardware and software components required to run

the experiment, a single stage readout using a large, dedicated local area network, driven by a central fast control system, which provides synchronous commands and timing. Wherever possible industry standard hardware and software are used and the number of different protocols and technologies is intenionally kept as small as possible.

Based on these principles the Online system of the current LHCb detector has been designed and commissioned. Fig. 3.4 gives a schematic overview. In this system data are pushed from the

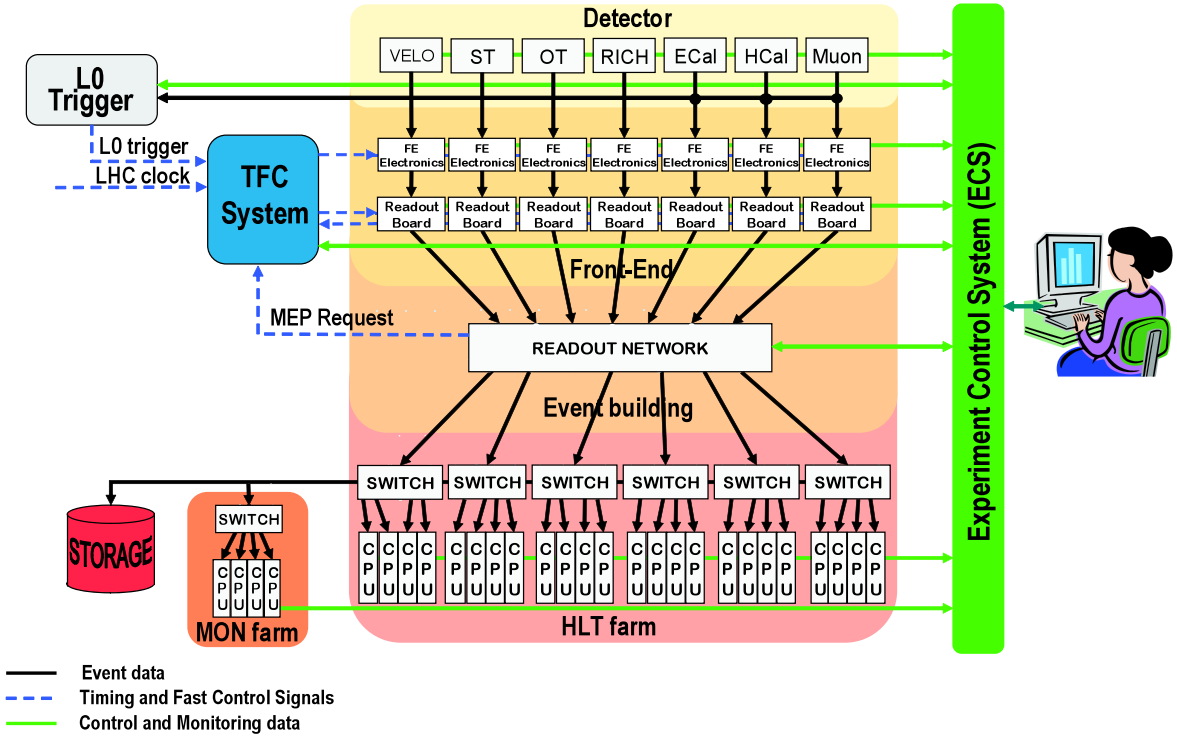


Figure 3.4: The LHCb Online system as from 2009. The individual components are explained in the text.

detector into the readout boards (TELL1/UKL1) shown at the top of the figure. The Timing and Fast Control (TFC) system, shown in the left upper part, broadcasts a destination address to the readout boards, which then send their data via the network, shown in the middle, to one of the computers in the event-filter farm (EFF) shown in the bottom. The computers in the EFF process the event data, select a small fraction of them and send these to the storage, shown at the lower left of the figure. The EFF computers then announce themselves to the TFC system as being available for new data, closing the cycle of data acquisition and high-level triggering.

All components are monitored and controlled by the experimental control system (ECS) indicated on the right-hand side of the figure.

While many components will need to be changed or upgraded, either to accommodate

the higher trigger-rate or naturally because of component obsolescence, the basic architectural choices described here briefly have been found to be successful and will be kept for the upgrade.

# Chapter 4

# Conclusion

The LHCb experiment is currently taking data successfully at the LHC. After the experiment has run for about five years at its design luminosity it is proposed to upgrade the experiment to run at higher luminosity. The upgraded detector is planned to be installed in the second long shutdown of the LHC machine, that is foreseen in the second half of this decade. Since the LHCb detector is spread out along the beam line, it is possible to work on several detectors at the same time, so that the total time for disassembly of the existing components and installation of the new ones is minimized. Nevertheless, in the first long shutdown we intend to do as much of the infrastructure work as possible in order to speed up the eventual installation.

The main focus of the upgrade is to increase the read-out of the experiment to 40 MHz, so that the increase in luminosity can be exploited with an improved trigger. All detector elements are needed to achieve full performance with the 40 MHz readout. A staging strategy has been developed that will allow individual elements to be installed when received and when installation time is available, so that experience can be gained in running them. This will be achieved by reading out all the detectors at the current 1 MHz readout rate, even if they have 40 MHz capabilities, until the upgrade installation is complete. The TORCH detector could be installed later if it is not available on time, with some impact on the particle identification performance at low momentum. R&D has started to verify the feasibility of this and other detector developments.

The physics case for the LHCb upgrade points to the compelling necessity for the experiment to measure the effects of any new particles seen by any of the LHC detectors. Such New Physics will require thorough study to identify and classify, and the upgraded LHCb would be the ideal experiment to perform this task using flavour physics observables, especially since $B_s$ decays are an important element of this work. The forward geometry, particle-identification capabilities and flexible trigger of the upgraded detector will also give LHCb unique and complementary capabilities in important topics beyond flavour physics.

The LHCb upgrade is necessary to take the next step in sensitivity that will be required in flavour physics after the first period of exploration and measurement that the experiment will perform over the coming five years. The sample sizes in most exclusive $B$ and $D$ final states will be far larger than those that will be collected elsewhere, for example at the upgraded $e^+e^-$ B-factories. The performance of the existing detector, and the purity of the samples already accumulated, gives confidence that measurements of very high sensitivity will be possible with these samples. The experiment will have no serious competition in its study of $B_s$ decays and

$CP$ violation.

The upgraded experiment will in addition have exciting opportunities to perform studies that will shed light on the lepton sector, and in topics beyond flavour physics. LHCb will be best-placed of all the LHC experiments to make an improved determination of $\sin^2\theta^{\rm lept}_{\rm eff}$, and to combat the PDF systematic uncertainties that may limit the ATLAS and CMS efforts to measure $m_W$. LHCb will have high sensitivity in the search for new particles with long lifetimes, and will be able to make QCD studies which are complementary to those possible in the central region.

That LHCb has taken data and demonstrated its abilities even under the challenging circumstances of many interactions per crossing, and is at a machine that will provide the needed luminosity, points to the LHCb Upgrade as being a golden opportunity for high energy physics.

# Bibliography


[1] H. Baer *et al.*, Phys. Rev. D**71** (2005) 095008; H. Baer *et al.*, JHEP **0507** (2005) 065; J.R. Ellis, K.A. Olive and P. Sandick, Phys. Rev. D **78** (2008) 075012.

[2] G.L. Bayatian *et al.* (CMS Collaboration), *CMS Technical Design Report, Volume II: Physics Performance*, CERN-LHCC-2006-021.

[3] O. Buchmueller *et al.*, arXiv:0907.5568 [hep-ph].

[4] T. Hurth and M. Nakao, Ann. Rev. Nucl. Part. Sci. **60** (2010) 645 [arXiv:1005.1224 [hep-ph]].

[5] J. Charles *et al.* (CKMfitter Group), Eur. Phys. J. C **41** (2005) 1 [arXiv:hep-ph/0406184]. Updated results and plots available online at `http://ckmfitter.in2p3.fr`

[6] M. Bona *et al.* (UTfit Collaboration), JHEP **0610** (2006) 081 [arXiv:hep-ph/0606167]. Updated results and plots available online at `http://www.utfit.org/`

[7] CDF public note 10206, `http://www-cdf.fnal.gov/physics/new/bottom/100513`; see also: T. Aaltonen *et al.* (CDF Collaboration), Phys. Rev. Lett. **100** (2008) 161802 [arXiv:0712.2397 [hep-ex]].

[8] D0 conference note 6098, `http://www-d0.fnal.gov/Run2Physics/WWW/results/`; see also: V. M. Abazov *et al.* (D0 Collaboration), Phys. Rev. Lett. **101** (2008) 241801 [arXiv:0802.2255 [hep-ex]].

[9] V. M. Abazov *et al.* (D0 Collaboration), Phys. Rev. D **82** (2010) 032001 [arXiv:1005.2757 [hep-ex]].

[10] V. M. Abazov *et al.* (D0 Collaboration), Phys. Rev. Lett. **105** (2010) 081801 [arXiv:1007.0395 [hep-ex]].

[11] B. Adeva, *et al.* (LHCb Collaboration), "Roadmap for selected key measurements of LHCb," arXiv:0912.4179 [hep-ex].

[12] R. Aaij *et al.* (LHCb Collaboration), Phys. Lett. B **694** (2010) 209 [arXiv:1009.2731 [hep-ex]].

[13] A. A. Alves Jr. *et al.* (LHCb Collaboration), "The LHCb Detector at the LHC", JINST **3** (2008) S08005.

[14] N. Cabibbo, Phys. Rev. Lett. **10** (1963) 531; M. Kobayashi and T. Maskawa, Prog. Theor. Phys. **49** (1973) 652.

[15] G. Buchalla *et al.*, Eur. Phys. J. C **57** (2008) 309 [arXiv:0801.1833 [hep-ph]].

[16] M. Antonelli *et al.*, Phys. Rept. **494** (2010) 197 [arXiv:0907.5386 [hep-ph]].

[17] G. D'Ambrosio, G. F. Giudice, G. Isidori and A. Strumia, Nucl. Phys. B **645** (2002) 155 [arXiv:hep-ph/0207036].

[18] G. Isidori, Y. Nir and G. Perez, arXiv:1002.0900 [hep-ph].

[19] A. Lenz *et al.*, arXiv:1008.1593 [hep-ph].

[20] S. R. Choudhury and N. Gaur, Phys. Lett. B **451** (1999) 86 [arXiv:hep-ph/9810307]; K. S. Babu and C. F. Kolda, Phys. Rev. Lett. **84** (2000) 228 [arXiv:hep-ph/9909476]; C. S. Huang, W. Liao, Q. S. Yan and S. H. Zhu, Phys. Rev. D **63** (2001) 114021 [Erratum-ibid. D **64** (2001) 059902] [arXiv:hep-ph/0006250].

[21] A. J. Buras, Prog. Theor. Phys. **122** (2009) 145 [arXiv:0904.4917 [hep-ph]].

[22] V. M. Abazov *et al.* (D0 Collaboration), Phys. Lett. B **693** (2010) 539 [arXiv:1006.3469 [hep-ex]].

[23] A. Soni, A. K. Alok, A. Giri, R. Mohanta and S. Nandi, Phys. Rev. D **82** (2010) 033009 [arXiv:1002.0595 [hep-ph]]; A. J. Buras, B. Duling, T. Feldmann, T. Heidsieck, C. Promberger and S. Recksiegel, JHEP **1009** (2010) 106 [arXiv:1002.2126 [hep-ph]]; W. S. Hou and C. Y. Ma, Phys. Rev. D **82** (2010) 036002 [arXiv:1004.2186 [hep-ph]].

[24] S. Nandi and A. Soni, arXiv:1011.6091 [hep-ph].

[25] I. Dunietz, R. Fleischer and U. Nierste, Phys. Rev. D **63** (2001) 114015 [arXiv:hep-ph/0012219].

[26] L. Wolfenstein, Phys. Rev. Lett. **51** (1983) 1945; A. J. Buras, M. E. Lautenbacher and G. Ostermaier, Phys. Rev. D **50** (1994) 3433 [arXiv:hep-ph/9403384].

[27] LHCb Collaboration, LHCb-CONF-2011-005.

[28] A. Lenz *et al.*, Phys. Rev. D 83, 036004 (2011) [arXiv:1008.1593 [hep-ph]].

[29] LHCb Collaboration, LHCb-CONF-2011-049.

[30] K. Nakamura *et al.*, (Particle Data Group), J. Phys. **G 37**, 075021 (2010)

[31] R. Aaij *et al.* (LHCb Collaboration), arXiv:1102.0206 [hep-ex], submitted to Phys. Lett. B.

[32] LHCb Collaboration, LHCb-CONF-2011-051.

[33] S. Stone and L. Zhang, Phys. Rev. D **79**, 074024 (2009) [arXiv:0812.2832 [hep-ph]].

[34] Y. Xie, P. Clarke, G. Cowan and F. Muheim, JHEP **0909**, 074 (2009) [arXiv:0908.3627 [hep-ph]].

[35] S. Faller, R. Fleischer and T. Mannel, Phys. Rev. D **79** (2009) 014005 [arXiv:0810.4248 [hep-ph]].

[36] K. De Bruyn, R. Fleischer and P. Koppenburg, arXiv:1012.0840 [hep-ph].

[37] R. Fleischer, Nucl. Phys. B **659** (2003) 321 [arXiv:hep-ph/0301256].

[38] A. Lenz and U. Nierste, JHEP **0706** (2007) 072 [arXiv:hep-ph/0612167].

[39] R. Aaij *et al.* (LHCb Collaboration), arXiv:1102.0348 [hep-ex], submitted to Phys. Lett. B.

[40] R. W. Lambert, CERN-THESIS-2009-001.

[41] N. Brook, N. Cottingham, R. W. Lambert, F. Muheim, J. Rademacker, P. Szczypka and Y. Xie, CERN-LHCB-2007-054.

[42] W. S. Hou, Phys. Rev. D **48** (1993) 2342; M. Tanaka, Z. Phys. C **67** (1995) 321 [arXiv:hep-ph/9411405]; K. Kiers and A. Soni, Phys. Rev. D **56** (1997) 5786 [arXiv:hep-ph/9706337].

[43] B. Grzadkowski and W. S. Hou, Phys. Lett. B **283** (1992) 427; R. Garisto, Phys. Rev. D **51** (1995) 1107 [arXiv:hep-ph/9403389]; C. H. Chen and C. Q. Geng, JHEP **0610** (2006) 053 [arXiv:hep-ph/0608166]; U. Nierste, S. Trine and S. Westhoff, Phys. Rev. D **78** (2008) 015006 [arXiv:0801.4938 [hep-ph]].

[44] LHCb Collaboration, LHCb-CONF-2011-011.

[45] Heavy Flavour Averaging Group, arXiv:1010.1589 [hep-ex], `http://www.slac.stanford.edu/xorg/hfag/`

[46] Y. Grossman and M. P. Worah, Phys. Lett. B **395** (1997) 241 [arXiv:hep-ph/9612269]; R. Fleischer, Int. J. Mod. Phys. A **12**, 2459 (1997) [arXiv:hep-ph/9612446]; D. London and A. Soni, Phys. Lett. B **407**, 61 (1997) [arXiv:hep-ph/9704277]; M. Ciuchini, E. Franco, G. Martinelli, A. Masiero and L. Silvestrini, Phys. Rev. Lett. **79** (1997) 978 [arXiv:hep-ph/9704274].

[47] M. Raidal, Phys. Rev. Lett. **89** (2002) 231803 [arXiv:hep-ph/0208091].

[48] M. Bartsch, G. Buchalla and C. Kraus, arXiv:0810.0249 [hep-ph]; M. Beneke, G. Buchalla, M. Neubert and C. T. Sachrajda, Nucl. Phys. B **591**, 313 (2000) [arXiv:hep-ph/0006124].

[49] N. Styles *et al.*, LHCb-PUB-2009-025.

[50] R. Fleischer, Phys. Rev. D **60** (1999) 073008 [arXiv:hep-ph/9903540]; M. Ciuchini, M. Pierini and L. Silvestrini, Phys. Rev. Lett. **100**, 031802 (2008) [arXiv:hep-ph/0703137].

[51] A. V. Gritsan and J. G. Smith, "Polarization in $B$ Decays," in Ref. [30]; H. Y. Cheng and J. G. Smith, Ann. Rev. Nucl. Part. Sci. **59** (2009) 215 [arXiv:0901.4396 [hep-ph]].

[52] N. G. Deshpande, N. Sinha and R. Sinha, Phys. Rev. Lett. **90** (2003) 061802 [arXiv:hep-ph/0207257]; M. Ciuchini, M. Pierini and L. Silvestrini, Phys. Rev. D **74** (2006) 051301 [arXiv:hep-ph/0601233]; M. Ciuchini, M. Pierini and L. Silvestrini, Phys. Lett. B **645** (2007) 201 [arXiv:hep-ph/0602207]; I. Bediaga, G. Guerrer and J. M. de Miranda, Phys. Rev. D **76** (2007) 073011.

[53] M. Gronau and D. London, Phys. Lett. B **253** (1991) 483; M. Gronau and D. Wyler, Phys. Lett. B **265** (1991) 172; D. Atwood, I. Dunietz and A. Soni, Phys. Rev. Lett. **78** (1997) 3257 [arXiv:hep-ph/9612433]; D. Atwood, I. Dunietz and A. Soni, Phys. Rev. D **63** (2001) 036005 [arXiv:hep-ph/0008090]; A. Giri, Y. Grossman, A. Soffer and J. Zupan, Phys. Rev. D **68** (2003) 054018 [arXiv:hep-ph/0303187].

[54] I. Dunietz, Phys. Lett. B **270** (1991) 75; M. Gronau, Phys. Lett. B **557** (2003) 198 [arXiv:hep-ph/0211282]; T. Gershon, Phys. Rev. D **79** (2009) 051301 [arXiv:0810.2706 [hep-ph]]; T. Gershon and M. Williams, Phys. Rev. D **80** (2009) 092002 [arXiv:0909.1495 [hep-ph]].

[55] R. Aleksan, I. Dunietz and B. Kayser, Z. Phys. C **54** (1992) 653.

[56] J. Shigemitsu, at CKM workshop 2010, Warwick
`http://indico.cern.ch/contributionDisplay.py?contribId=3&confId=96378`

[57] A. J. Buras, M. V. Carlucci, S. Gori and G. Isidori, JHEP **1010** (2010) 009.

[58] J. R. Ellis, K. A. Olive and V. C. Spanos, Phys. Lett. B **624** (2005) 47 [arXiv:hep-ph/0504196].

[59] R. Aaij *et al.* (LHCb Collaboration), Phys. Lett. B **699** (2011) 330, [arXiv:1103.2465], CERN-PH-EP-2011-029.

[60] CDF Collaboration, CDF Public Note 9892.

[61] V. Abazov *et al.*, (D0 Collaboration), Phys. Lett. B **693** (2010) 539.

[62] LHCb Collaboration, LHCb-CONF-2011-037.

[63] R. Hodgkinson and A. Pilaftsis, Phys. Rev. D **78** (2008) 075004.

[64] P. Urquijo, "Open charm and beauty production at LHCb," presented at "Charm and bottom quark production at the LHC," CERN, Dec. 3, 2010, `http://indico.cern.ch/conferenceOtherViews.py?view=standard&confId=111524`

[65] R. Fleischer, N. Serra and N. Tuning, Phys. Rev. D **82** (2010) 034038 [arXiv:1004.3982 [hep-ph]]; R. Fleischer, N. Serra and N. Tuning, arXiv:1012.2784 [hep-ph].

[66] T. Hurth, G. Isidori, J. F. Kamenik and F. Mescia, Nucl. Phys. B **808**, 326 (2009) [arXiv:0807.5039 [hep-ph]]; W. Altmannshofer, A. J. Buras, S. Gori, P. Paradisi and D. M. Straub, Nucl. Phys. B **830** (2010) 17 [arXiv:0909.1333 [hep-ph]].

[67] T. Aaltonen *et al.* (CDF Collaboration) Phys. Rev. Lett. **103** (2009) 031801 [arXiv:0812.4271 [hep-ex]].

[68] M. Beneke, T. Feldmann and D. Seidel, Nucl. Phys. B **612** (2001) 25 [arXiv:hep-ph/0106067]; M. Beneke, T. Feldmann and D. Seidel, Eur. Phys. J. C **41** (2005) 173 [arXiv:hep-ph/0412400].

[69] B. Aubert *et al.* (BABAR Collaboration), Phys. Rev. D **79** (2009) 031102 [arXiv:0804.4412 [hep-ex]]; J. T. Wei *et al.* (BELLE Collaboration), Phys. Rev. Lett. **103** (2009) 171801 [arXiv:0904.0770 [hep-ex]]; T. Aaltonen *et al.* (CDF Collaboration), arXiv:1101.1028 [hep-ex].

[70] LHCb Collaboration, LHCb-CONF-2011-038.

[71] C. Bobeth, G. Hiller, and D. van Dyk, "More Benefits of Semileptonic Rare B Decays at Low Recoil: CP Violation", arXiv:1105.0376, 2011.

[72] F. Kruger and J. Matias, Phys. Rev. D **71** (2005) 094009 [arXiv:hep-ph/0502060]; W. Altmannshofer, P. Ball, A. Bharucha, A. J. Buras, D. M. Straub and M. Wick, JHEP **0901** (2009) 019 [arXiv:0811.1214 [hep-ph]]; A. K. Alok, A. Dighe, D. Ghosh, D. London, J. Matias, M. Nagashima and A. Szynkman, JHEP **1002** (2010) 053 [arXiv:0912.1382 [hep-ph]]; U. Egede, T. Hurth, J. Matias, M. Ramon and W. Reece, JHEP **1010** (2010) 056 [arXiv:1005.0571 [hep-ph]].

[73] U. Egede, T. Hurth, J. Matias, M. Ramon and W. Reece, JHEP **0811** (2008) 032 [arXiv:0807.2589 [hep-ph]].

[74] C. Bobeth, T. Ewerth, F. Kruger and J. Urban, Phys. Rev. D **64** (2001) 074014 [arXiv:hep-ph/0104284]; C. Bobeth, G. Hiller and G. Piranishvili, JHEP **0712** (2007) 040 [arXiv:0709.4174 [hep-ph]].

[75] Q. S. Yan, C. S. Huang, W. Liao and S. H. Zhu, Phys. Rev. D **62** (2000) 094023 [arXiv:hep-ph/0004262]; G. Hiller and F. Kruger, Phys. Rev. D **69** (2004) 074020 [arXiv:hep-ph/0310219].

[76] D. Atwood, M. Gronau and A. Soni, Phys. Rev. Lett. **79**, 185 (1997) [arXiv:hep-ph/9704272]; D. Atwood, T. Gershon, M. Hazumi and A. Soni, Phys. Rev. D **71** (2005) 076003 [arXiv:hep-ph/0410036].

[77] F. Muheim, Y. Xie and R. Zwicky, Phys. Lett. B **664** (2008) 174 [arXiv:0802.0876 [hep-ph]].

[78] D. Melikhov, N. Nikitin and S. Simula, Phys. Lett. B **442** (1998) 381 [arXiv:hep-ph/9807464]; Y. Grossman and D. Pirjol, JHEP **0006** (2000) 029 [arXiv:hep-ph/0005069].

[79] M. Gronau, Y. Grossman, D. Pirjol and A. Ryd, Phys. Rev. Lett. **88** (2002) 051802 [arXiv:hep-ph/0107254]; M. Gronau and D. Pirjol, Phys. Rev. D **66** (2002) 054008 [arXiv:hep-ph/0205065]; E. Kou, A. L. Yaouanc and A. Tayduganov, arXiv:1011.6593 [hep-ph].

[80] D. Atwood, T. Gershon, M. Hazumi and A. Soni, arXiv:hep-ph/0701021; V. D. Orlovsky and V. I. Shevchenko, Phys. Rev. D **77** (2008) 093003 [arXiv:0708.4302 [hep-ph]].

[81] C. D. Lu, Eur. Phys. J. C **24**, 121 (2002) [arXiv:hep-ph/0112127].

[82] L. Hofer, D. Scherer and L. Vernazza, arXiv:1011.6319 [hep-ph].

[83] D. Pirjol and J. Zupan, JHEP **1002** (2010) 028 [arXiv:0908.3150 [hep-ph]].

[84] I. I. Bigi, M. Blanke, A. J. Buras and S. Recksiegel, JHEP **0907** (2009) 097; Y. Grossman, Y. Nir and G. Perez, Phys. Rev. Lett. **103** (2009) 071602; M. Bauer, S. Casagrande, U. Haisch and M. Neubert, JHEP **1009** (2010) 017.

[85] Y. Grossman, A. L. Kagan and Y. Nir, Phys. Rev. D **75** (2007) 036008 [arXiv:hep-ph/0609178].

[86] I. Bediaga, I.I. Bigi, A. Gomes, G. Guerrer, J. Miranda, A.C. dos Reis *et al.*, Phys. Rev. D **80**, 096006 (2009).

[87] I.I. Bigi, in Proceedings of KAON2001: International Conference on CP violaton, Pisa, Italy, 12-17 June 2001, p. 417 (hep-ph/0107102).

[88] A. Bondar, A. Poluektov and V. Vorobiev, Phys. Rev. D **82**, 034033 (2010).

[89] J. Libby *et al.* (CLEO Collaboration), "Model-independent determination of the strong-phase difference between $D^0$ and $\bar{D}^0 \to K^0_{S,L}h^+h^-$ ($h = \pi, K$) and its impact on the measurement of the CKM angle $\gamma/\phi_3$ ", arXiv:1010.2817 [hep-ex].

[90] M. Petric *et al.* (Belle Collaboration), Phys. Rev. D **81**, 091102(R) (2010).

[91] G. Burdman, E. Golowich, J. Hewett and S. Pakvasa, Phys. Rev. D **66**, 014009 (2002).

[92] I. Dorsner, S. Fajfer, J. F. Kamenik and N. Kosnik, Phys. Lett. **B682**, 67 (2009).

[93] J.C. Pati and A. Salam, Phys. Rev. **D10** (1974) 275; R.N. Mohapatra and J.C. Pati, Phys. Rev. **D 11** (1975) 566, 2558; G. Senjanovic and R.N. Mohapatra, Phys. Rev. **D 12** (1975) 1502.

[94] N. Arkani-Hamed, S. Dimopoulos, G. Dvali and J. March-Russel, Phys. Rev. **D 65** (2002) 024032; Y. Grossman and M. Neubert, Phys. Lett. **B 474** (2000) 361; K. R. Dienes and I. Sarcevic, Phys. Lett. **B 500** (2001) 133; S.J. Huber and Q. Shafi, Phys. Lett. **B 544** (2002) 295; G. Perez and L. Randall, JHEP 01 (2009) 077.

[95] T. Asaka and M. Shaposhnikov, Phys. Lett. **B 620** (2005) 17; T. Asaka, S. Blanchet and M. Shaposhnikov, Phys. Lett. **B 631** (2005) 151; F. Bezrukov, D. Gorbunov, JHEP **1005** (2010) 010. [arXiv:0912.0390 [hep-ph]]; A. Roy, M. Shaposhnikov, Phys. Rev. **D82** (2010) 056014. [arXiv:1006.4008 [hep-ph]].

[96] A. Boyarsky, O. Ruchayskiy and M. Shaposhnikov, Ann. Rev. Nucl. Part. Sci. **59** (2009) 191 [arXiv:0901.0011 [hep-ph]]

[97] M. Shaposhnikov, JHEP **0808** (2008) 008 [arXiv:0804.4542 [hep-ph]].

[98] A. Atre, T. Han, S. Pascoli, and B. Zhang, JHEP, 0905:030 (2009) [arXiv:0901.3589]; A. Atre, V. Barger and T. Han, Phys. Rev. D**71**, 113014 (2005) [arXiv:hep-ph/0502163].

[99] J.-M. Zhang, and G.-L. Wang, arXiv:1003.5570 [hep-ph].

[100] D. Gorbunov and M. Shaposhnikov, JHEP **0710** (2007) 015 [arXiv:0705.1729 [hep-ph]].

[101] A. M. Cooper-Sarkar *et al.* (WA66 Collaboration), Phys. Lett. B **160** (1985) 207; F. Bergsma *et al.* (CHARM Collaboration), Phys. Lett. B **166** (1986) 473; G. Bernardi *et al.*, Phys. Lett. B **166** (1986) 479; G. Bernardi *et al.*, Phys. Lett. B **203** (1988) 332; A. Vaitaitis *et al.* (NuTeV Collaboration), Phys. Rev. Lett. **83** (1999) 4943.

[102] L. Canetti and M. Shaposhnikov, arXiv:1006.0133 [hep-ph].

[103] B. Aubert *et al.* (BABAR Collaboration), Phys. Rev. Lett. **104** (2010) 021802 [arXiv:0908.2381 [hep-ex]]; K. Hayasakai *et al.* (Belle Collaboration),' Phys. Lett. B **687** (2010) 139 [arXiv:1001.3221 [hep-ex]].

[104] B. O'Leary *et al.* (SuperB Collaboration), arXiv:1008.1541 [hep-ex].

[105] H. K. Dreiner, M. Kramer and B. O'Leary, Phys. Rev. D **75**, 114016 (2007) [arXiv:hep-ph/0612278]; M. Raidal *et al.*, Eur. Phys. J. C **57**, 13 (2008) [arXiv:0801.1826 [hep-ph]].

[106] Y. Miyazaki*et al.* (Belle Collaboration), Phys. Lett. B **682**, 355 (2010) [arXiv:0908.3156 [hep-ph]].

[107] The ALEPH, DELPHI, L3, OPAL, SLD Collaborations, the LEP Electroweak Working Group, the SLD Electroweak and Heavy Flavour Group, Phys. Reports **427** 5-6 (2006) 257, hep-ex/0509008.

[108] V. Buge *et al.* (CMS Collaboration), J. Phys. **G 34** (2007) 995; N. Besson *et al.*, arXiv:0805.2093 [hep-ex].

[109] M.W. Krasny, F. Dydak, F. Fayette, W. Placzek and A. Siodmok, Eur. Phys. J. C69 (2010) 379, arXiv:1004.2597 [hep-ex].

[110] K. Zurek, "TASI 2009 Lectures: Searching for Unexpected Physics at the LHC," arXiv:1001.2563v1 [hep-ph].

[111] M. Cvetic, P. Langacker and G. Shiu, Phys. Rev. D **66**, 066004 (2002) [hep-ph/0205252], and references therein; N. Arkani-Hamed, S. Dimopoulos and S. Kachru, [hep-th/0501082]; V. Barger, P. Langacker and G. Shaughnessy, [hep-ph/0702001].

[112] M. J. Strasser and K. M. Zurek, Phys. Lett. B **651**, 374 (2007) [hep-ph/0604261].

[113] M. J. Strasser and K. M. Zurek, Phys. Lett. B **661**, 263 (2008) [hep-ph/0605193].

[114] F. de Campos, O. J. P. Eboli, M. B. Magro, and D. Restrepo, Phys. Rev. D **79**, 055008 (2009)

[115] L. Carpenter, D. Kaplan, and E.-J. Rhee, Phys. Rev. Lett. 99, 211801, (2007) [hep-ph/0607204].

[116] T. Aaltonen *et al.* (CDF Collaboration), Phys. Rev. Lett. **99** (2007) 242002.

[117] T. Aaltonen *et al.* (CDF Collaboration), Phys. Rev. **D 77** (2008) 052004; V. Abazov *et al.* (D0 Collaboration), arXiv:1009.2444 [hep-ex].

[118] T. Aaltonen *et al.* (CDF Collaboration), Phys. Rev. Lett. **102** (2009) 242001.

[119] `http://projects.hepforge.org/superchic`

[120] J.W. Lämsaä and R. Orava, 2009 JINT **4** P11019.

[121] M. Albrow *et al.*, JINST **4** (2009) T10001.

[122] L.A. Harland-Lang, V.A. Khoze, M.G. Ryskin and W.J. Stirling, Eur. Phys. J. **C 69** (2010) 179.

[123] S. Heinemeyer, V.A. Khoze, M.G. Ryskin, M. Tasevesky and G. Weiglein, arXiv:1012.5007 [hep-ph].

[124] L.A. Harland-Lang, V.A. Khoze, M.G. Ryskin and W.J. Stirling, arXiv:1011.0680 [hep-ph].

[125] E. Aslanides *et al.*, Nucl. Instrum. And Meth. A 579 (2007) 989.

[126] J. Albrecht, L. de Paula, A. Pérez-Calero Yzquierdo and F. Teubert, "Commissioning and performance of the LHCb HLT1 muon trigger", LHCb-PUB-2011-006.

[127] V. Gligorov, "A single track HLT1 trigger", LHCb-PUB-2011-003.

[128] M. Williams *et al.*, "The HLT2 topological lines", LHCb-PUB-2011-002.

[129] J. Christiansen, "Requirements to the L0 front-end electronics", LHCb Technical Note, LHCb 2001-014.

[130] M. Campbell, "10 years of the Medipix2 collaboration", Nucl. Instrum. and Meth. A, in print.

[131] P. Collins et. al., "The LHCb VELO Upgrade", Nucl. Instrum. and Meth. **A** 51628.

[132] K. Kirsebom *et al.* (LHCb Collaboration), LHCb Letter of Intent: "A Dedicated LHC Collider Beauty Experiment for Precision Measurements of CP-Violation", CERN/LHCC 95-5, 25 August 1995.

[133] S. Amato *et al.* (LHCb Collaboration), LHCb Technical proposal: "A Large Hadron Collider Beauty Expriment for Precision Measurements of CP-Violation and Rare Decays", CERN/LHCC 98-4, 20 February 1998.

[134] R.A. Nobrega *et al.* (LHCb Collaboration), Technical Design Report: "LHCb Reoptimized Detector and Performance", [CERN-LHCC 2002-029], 8 November 2002.

[135] S. Amato *et al.* (LHCb Collaboration), "LHCb RICH Technical Design Report", CERN LHCC 2000-037 (2000).

[136] M. Charles and R. Forty, "TORCH: time-of-flight identification with Cherenkov radiation", proceedings of RICH2010, to be published in Nucl. Instrum. Meth. A, arXiv:1009.3793v1 [physics.ins-det].

[137] B. Aubert *et al.* (BABAR Collaboration), Nucl. Instrum. and Meth. A **479** (2002) 1.

[138] S. Amato *et al.* (LHCb Collaboration), "LHCb calorimeters technical design report", CERN-LHCC-2000-036.

[139] The LHCb Collaboration, "LHCb Muon System Technical Design Report", CERN/LHCC 2001-010 and "Addendum to LHCb Muon System Technical Design Report", CERN/LHCC 2003-002.

[140] M. Anelli *et al.*, "Performance of the LHCb muon system with cosmic rays", JINST 5:P10003, 2010.

[141] P.R. Barbosa-Marinho *et al.*, "LHCb Online system technical design report: Data acquisition and experiment control", CERN-LHCC-2001-040.